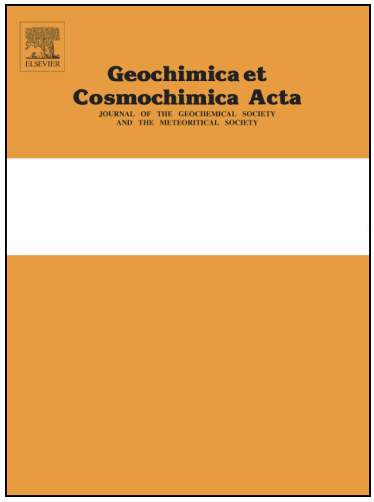

Clumped Isotope Thermometry Of Calcite And Dolomite In A Contact Metamorphic Environment

Max K. Lloyd, John M. Eiler, Peter I. Nabelek

PII: S0016-7037(16)30615-9
DOI: http://dx.doi.org/10.1016/j.gca.2016.10.037
Reference: GCA 9992

To appear in: *Geochimica et Cosmochimica Acta*

Received Date: 23 March 2016
Revised Date: 19 October 2016
Accepted Date: 23 October 2016

Please cite this article as: Lloyd, M.K., Eiler, J.M., Nabelek, P.I., Clumped Isotope Thermometry Of Calcite And Dolomite In A Contact Metamorphic Environment, *Geochimica et Cosmochimica Acta* (2016), doi: http://dx.doi.org/10.1016/j.gca.2016.10.037

CLUMPED ISOTOPE THERMOMETRY OF CALCITE AND DOLOMITE IN A CONTACT METAMORPHIC ENVIRONMENT

MAX K. LLOYD[a*], JOHN M. EILER[a], AND PETER I. NABELEK[b]

*Corresponding author: mlloyd@caltech.edu; a) Division of Geological and Planetary Sciences, California Inst. of Technology, Pasadena, CA 91125; b) Department of Geological Sciences, University of Missouri, Columbia, MO 65211-1380

ABSTRACT

Clumped isotope compositions of slowly-cooled calcite and dolomite marbles record apparent equilibrium temperatures of roughly 150-200 °C and 300-350 °C, respectively. Because clumped isotope compositions are sensitive to the details of T-t path within these intervals, measurements of the Δ_{47} values of coexisting calcite and dolomite can place new constraints on thermal history of low-grade metamorphic rocks over a large portion of the upper crust (from ~5 to ~15 km depth). We studied the clumped isotope geochemistry of coexisting calcite and dolomite in marbles from the Notch Peak contact metamorphic aureole, Utah. Here, flat-lying limestones were intruded by a pluton, producing a regular, zoned metamorphic aureole. Calcite Δ_{47} temperatures are uniform, 156 ± 12 ˚C (2σ s.e.), across rocks varying from high-grade marbles that exceeded 500 °C to nominally unmetamorphosed limestones >5 km from the intrusion. This result appears to require that the temperature far from the pluton was close to this value; an ambient temperature just 20 ˚C lower would not have permitted substantial re-equilibration, and should have preserved depositional or early diagenetic Δ_{47} values several km from the pluton.

Combining this result with depth constraints from overlying strata suggests the country rock here had an average regional geotherm of 22.3–27.4 ˚C/km from the late Jurassic Period until at least the middle Paleogene Period. Dolomite Δ_{47} in all samples above the talc+tremolite-in isograd record apparent equilibrium temperatures of 328^{+13}_{-12} °C (1σ s.e.), consistent with the apparent equilibrium blocking temperature we expect for cooling from peak metamorphic conditions. At greater distances, dolomite Δ_{47} records temperatures of peak (anchi)metamorphism or pre-metamorphic diagenetic conditions. The interface between these domains is the location of the 330 ˚C isotherm associated with intrusion. Multiple-phase clumped isotope measurements are complemented by bulk $\delta^{13}C$ and $\delta^{18}O$ dolomite-calcite thermometry. These isotopic exchange thermometers are largely consistent with peak temperatures in all samples within 4 km of the contact, indicating that metamorphic recrystallization can occur even in samples too low-grade to produce growth of conventional metamorphic index minerals (i.e., talc and tremolite). Altogether, this work demonstrates the potential of these methods to quantify the conditions of metamorphism at sub-greenschist facies.

1. INTRODUCTION

There are relatively few quantitative geothermometers that can be used to investigate the thermal histories and temperatures of chemical processes occurring in the upper ~15 km of the crust. Below ~300 °C, most heterogeneous

equilibria, including the cation and stable isotope exchange reactions upon which most geothermometers are based, proceed too slowly to reach thermodynamic equilibrium. Some established thermometers, such as oxygen isotope fractionation in quartz–calcite veins (Kirschner et al., 1995) or fluid inclusion phase equilibria and microthermometry (Mullis et al., 1994), are applicable in this range of relatively low temperatures, but only to narrow types of samples. Other methods are more widely applicable but yield only semi-quantitative constraints, such as a relative ranking of thermal maturity (e.g., illite crystallinity; conodont color alteration; vitrinite reflectance; Frey, 1987). One method of thermometry that might seem to offer a useful approach to shallow crustal settings — the carbonate–water oxygen isotope thermometer (which rapidly equilibrates at most diagenetic and low-grade metamorphic conditions; Epstein et al., 1953) is rarely useful because one generally lacks precise constraints on the $\delta^{18}O$ of crustal waters (Sheppard, 1986).

Carbonate clumped isotope thermometry offers a relatively new approach to determine the thermal histories of surface and shallow crustal processes (see review by Eiler, 2011). Because it is based on a homogeneous equilibrium recorded by the carbonate mineral lattice, and carbonates appear to often grow at or near isotopic equilibrium, it is potentially useful (as good as est. ±10 ˚C) as a recorder of crustal processes up to ~300 ˚C. While most uses of this technique have focused on paleoclimate problems using biogenic and soil carbonates, proof-of-concept studies have already demonstrated its usefulness for the study

of early diagenesis (Huntington et al., 2011), dolomitization (Ferry et al., 2011), cementation (Dale et al., 2014), and hydrothermal alteration at temperatures relevant to the shallow crust (Bristow et al., 2011).

Carbonate clumped isotope thermometry in sub-surface environments is complicated because apparent temperatures may be modified by solid state diffusion, which re-orders bonds between rare isotopes on geologic timescales (Dennis and Schrag, 2010). Studies of C-O bond reordering kinetics in calcite predict that measurable resetting should occur at temperatures as low as ~115 °C on timescales of hundreds of millions of years (Henkes et al., 2014; Passey and Henkes, 2012; Stolper and Eiler, 2015). Moreover, the exact clumped isotope composition preserved in a crystal, and the degree to which it is reset from an initial value, can depend on the specific T-t path through the window where C-O reordering can occur. This phenomenon presents a problem for the interpretation of paleoclimate records in deeply buried samples, but also presents an opportunity for a new tool to study the thermal histories of rocks — a 'clumped isotope geospeedometry' — i.e., the constraint of cooling rate (or other features of a cooling history) based on the preservation of apparent temperatures. This concept has been successfully employed in some initial studies to predict the cooling rate of a metamorphic core complex (Passey and Henkes, 2012), the maximum burial depths of carbonate fossils in depositional basins (Henkes et al., 2014; Shenton et al., 2015) and the geotherm traversed by buried and exhumed soils (Stolper and Eiler, 2015).

Here we examine the clumped isotope systematics of calcite and dolomite in a contact metamorphic environment, compare these results with the heterogeneous C and O isotope exchange equilibria between these two minerals, and interpret these findings with respect to experimental determinations of the kinetics of clumped isotope re-ordering and intermineral exchange of stable isotopes. To the best of our knowledge, this is the first study to integrate constraints from multiple simultaneous clumped isotope equilibria with each other and with more conventional stable isotope geothermometers. Our purpose is both to illuminate the thermal history surrounding a shallow crustal intrusion, including locations and times that are poorly constrained by other techniques, and to illustrate a general methodology that may be helpful in studying thermal histories of other metamorphic settings.

2. BACKGROUND

The formation of bonds between the rare, heavy isotopes of C and O in carbonates (i.e., ^{13}C–^{18}O bearing carbonate ion groups) is governed by the thermodynamic balance between minimization of vibrational energy (lowest when heavy isotopes are bonded to each other), and maximization of configurational entropy (highest when all carbon and oxygen isotopes are randomly distributed among all isotopologues of CO_3^{-2} — a state referred to as the stochastic distribution). This balance can be expressed by the isotope exchange reaction (for calcite):

$Ca^{13}C^{16}O_3 + Ca^{12}C^{18}O^{16}O_2 = Ca^{12}C^{16}O_3 + Ca^{13}C^{18}O^{16}O_2$. Reaction 1

The equilibrium constant for this reaction, K_{eq1}, is measured by digestion of a carbonate phase in phosphoric acid and analysis of the isotopic composition of the evolved CO_2 by sector mass spectrometry (or potentially other methods, such as absorption spectroscopy); the essential point here is that the proportion of ^{13}C–^{18}O bonds in the evolved CO_2 is fractionated by acid digestion but (apparently) not re-equilibrated by exchange. Thus, just as for an acid-digestion measurement of the $\delta^{18}O$ of carbonates, one can indirectly observe the state of isotopic ordering in reactant $(CO_3)_2$ groups by observing that in the product CO_2 molecules. The degree to which multiple isotopic substitution — or isotopic "clumping" — is present in a sample of CO_2 is expressed as:

$$\Delta_{47} = \left[\left(\frac{R^{47}}{R^{47*}} - 1 \right) - \left(\frac{R^{46}}{R^{46*}} - 1 \right) - \left(\frac{R^{45}}{R^{45*}} - 1 \right) \right] \times 1000,$$

where R^{47}, R^{46}, and R^{45} are the measured intensity ratios of masses 47, 46, and 45 over mass 44, respectively, of the evolved CO_2, and the * denotes the expected value for a ratio given a stochastic distribution of isotopes among all isotopologues (Eiler and Schauble, 2004; Ghosh et al., 2006; Wang et al., 2004). Because K_{eq1} in carbonate is temperature-dependent, the measured

Δ_{47} value of CO_2 evolved from that carbonate depends on the growth temperature (assuming the carbonate grew at or near equilibrium with respect to reaction 1).

2.1 THE KINETICS OF CLUMPED ISOTOPE REORDERING IN CARBONATE

If a crystal is not in clumped isotopic equilibrium with its ambient temperature, the clumped isotope composition can evolve toward equilibrium by C–O bond reordering, provided atomic mobility allows migration of isotopes among nearby crystal sites (Passey and Henkes, 2012). The exact mechanism for this reordering is unclear, but likely involves the breakage of C-O bonds and subsequent reformation using C and O from neighboring carbonate groups or interstitial positions within the crystal lattice (Henkes et al., 2014). Calcite Δ_{47} reordering exhibits non-first order behavior in laboratory heating experiments (Passey and Henkes, 2012; Henkes et al., 2014; Stolper and Eiler, 2015). Specifically, when heating a relatively high-Δ_{47} calcite crystal, C–O bonds reorder toward a stochastic distribution rapidly but incompletely during the first few hours, after which the rate of re-equilibration slows. Henkes et al. (2014) attribute the rapid reordering to diffusion along crystallographic defects that can be annealed at high temperature. Once these 'transient' structural or point defects are eliminated, reordering occurs solely using unannealable defects, such as intrinsic defects or ionic impurities (Henkes et al., 2014). Stolper and Eiler (2015)

hypothesize that the similarity in reordering behavior among different calcite samples, and the observation of the same behavior in a second phase (apatite), suggests that it reflects something intrinsic and universal to the kinetics of clumped isotope reordering rather than an idiosyncrasy of deformational or other defects. These authors fit the experimental data by simultaneously solving two first order linear differential equations for two reaction rate constants. The physical justification for this model is that C–O bond reordering occurs in two steps: (1) isotopic exchange between neighboring carbonate groups, and (2) diffusion of carbonate groups through the crystal lattice. When a relatively high-Δ_{47} carbonate is heated, such that it has an excess of ^{13}C–^{18}O bonds compared to equilibrium at its new condition, rapid initial reordering occurs through division of the clumped isotopologues to form two neighboring carbonate groups that each possess one rare isotope. However, these adjacent species effectively create a population of domains within the crystal that are enriched in both ^{13}C and ^{18}O, which readily re-exchange with each other to maintain a high overall abundance of clumped species. This can be thought of as a special case of well known 'mixing' effects, where mixing two populations that differ in bulk isotopic composition but share a state of isotopic ordering results in a mixture with an excess of 'clumps' (Eiler and Schauble, 2004; Eiler 2007, 2013). Further decline in the abundance of clumped species depends on the migration of ^{13}C and ^{18}O away from each other by the slower process of diffusion through the crystal lattice.

Although the models of Henkes et al. (2014) and Stolper and Eiler (2015) are calibrated to describe statistically indistinguishable data, their distinct theoretical groundings lead to discrepancies in how they should be applied to the case of a high-grade marble undergoing slow cooling. Since the calcite crystals in this marble are formed above the temperature where Henkes et al. (2014) suggest transient defects anneal, only the slower, 'post-annealing' reordering kinetics should be considered when modeling the change in Δ_{47} with cooling. According to the Stolper and Eiler (2015) model, however, the rapid reordering phase is an intrinsic property of the crystal lattice, and should not be annealed even when a sample is crystallized at high temperatures. This difference is subtle for all natural carbonates measured so far, but could be significant for a material with exceptionally large capacity for reordering via the rapid mechanism (i.e., a high concentration of pairs or transient defects, depending on the model). It is not yet known whether one, both, or neither of these models accurately describe clumped isotope re-ordering kinetics in natural materials. Both models predict apparent equilibrium blocking temperatures in calcite of 150–200 °C, which are consistent with measurements of slowly cooled marbles (Eiler, 2011; Passey and Henkes, 2012). The apparent equilibrium blocking temperature should be dependent on the cooling rate near this temperature; initial measurements suggest that this dependence has been observed (Stolper and Eiler, 2015). Apparent equilibrium blocking temperatures in dolomitic marbles are 300–350 °C (Ferry et al., 2011; Supplementary Table S4), which suggest that the carbonate clumped isotope reordering kinetics in dolomite are slower than in calcite (Fig. 1).

2.2 DOLOMITE–CALCITE STABLE ISOTOPE EXCHANGE REACTIONS

Although the focus of this study is the clumped isotope geochemistry of co-existing calcite and dolomite in metamorphic rocks, these measurements are complemented by simultaneously considering fractionations of carbon and oxygen isotopes between co-existing calcite and dolomite. These fractionations are temperature-dependent when controlled by equilibrium thermodynamics, and have been demonstrated to be effective thermometers (Sheppard and Schwarcz, 1970). At thermodynamic equilibrium, dolomite is higher in $\delta^{13}C$ and $\delta^{18}O$ than co-existing calcite, by amounts that vary from ~0.5 to 1.5‰ ($\delta^{13}C$) and from ~0.5 to 2.5‰ ($\delta^{18}O$) at temperatures from ~700 to 200 °C, respectively. Theoretical predictions of these fractionations (Chacko and Deines, 2008; Deines, 2004; Schauble et al., 2006) are in general agreement with both laboratory experiments (Horita, 2014; Matthews and Katz, 1977), and observations of a suite of natural meta-limestones from the Chester dome area, Vermont, USA (Sheppard and Schwarcz, 1970). It is worth noting, however, that natural dolomite–calcite isotope fractionations are highly scattered when a wide diversity of rocks are considered, likely due to the failure to attain and/or preserve local equilibrium at the scale of analysis (Ferry et al., 2010). In addition, in environments where H_2O-rich fluids react with carbonate rocks, variable amounts of water–mineral exchange and isotopic fractionations due to decarbonation reactions may disturb originally equilibrated intermineral fractionations (Labotka et al., 2011).

The solid-state diffusion rates of oxygen and carbon in calcite and dolomite suggest that stable isotope exchange equilibria between these minerals should have higher apparent equilibrium blocking temperatures than the clumped isotope thermometers (Anderson, 1972; Farver, 1994; Labotka et al., 2011; Fig. 1). At geologically rapid cooling rates in dry environments, calcite grains hundreds of microns across are effectively closed to diffusion-limited changes in bulk isotopic composition at temperatures below 600 °C (Labotka et al., 2011). Water fugacity has a strong effect on oxygen diffusivity, lowering the apparent equilibrium blocking temperature by as much as 150 °C in pure H_2O (Farver, 1994; Labotka et al., 2011). (It is interesting to note that despite the effect of f_{H2O} on oxygen and carbon diffusivity, to date no effect of f_{H2O} on clumped isotope reordering rate has been observed; Passey and Henkes, 2012.) The experimentally determined self-diffusion rates of C and O in calcite (in the case of O, assuming a value of f_{H2O}) can be used to estimate the blocking temperatures of C and O exchange between coexisting calcite and dolomite (Lasaga, 1998; Fig. 1). The rates of C and O self-diffusion in dolomite are poorly understood, but one published study suggests that they are more rapid than in calcite at comparable conditions (Anderson, 1972). Therefore, our calculations assume that diffusion through calcite is the rate-limiting step to dolomite–calcite isotopic re-equilibration (note that this assumption may be invalid in rocks containing much more calcite than dolomite, or in which calcite is far finer grained than dolomite; Eiler et al., 1992). These calculations show that in contact metamorphic environments with relatively high X_{CO_2} values (>0.5, consistent with the unit of interest in this study), low f_{H2O} (tens of MPa,

appropriate for the unit), and relatively rapid cooling rate (>100 °C/Ma), the dolomite–calcite oxygen and carbon isotope exchange thermometers are expected to have apparent equilibrium blocking temperatures on the order of 550–700 °C (Fig. 1). It should be noted, however, that if isotopic self-diffusion in dolomite is faster than in calcite, dolomite could continue to equilibrate with a pore fluid (or other co-existing phase) to a lower temperature.

2.3 THE STABLE ISOTOPE SYSTEMATICS OF CONTACT METAMORPHISM OF CARBONATES

Here we examine the expected stable isotope systematics (including both clumped isotope and heterogeneous isotope exchange equilibria) for carbonates that undergo a metamorphic event broadly resembling that experienced in shallow crustal contact metamorphic settings. A key question for models of stable isotope systematics associated with metamorphism of carbonates is whether the rate-limiting step for setting the isotopic composition of a mineral grain is atomic mobility through a pre-existing mineral lattice (i.e., inter- or intra-crystalline diffusion), or any of the several processes of mineral growth (recrystallization by grain coarsening or dissolution/reprecipitation; new mineral growth associated with a metamorphic reaction, for example calcite formed by the talc-in reaction, dolomite+quartz+water = calcite+talc+CO_2). Diffusion-controlled processes only permit rapid and complete changes in isotopic composition when ambient temperatures exceed the blocking

temperature, whereas processes of mineral growth should be expected to equilibrate the new mineral with grain boundary fluid and other newly forming minerals essentially instantaneously (i.e., because the kinetics of isotopic exchange of dissolved inorganic carbonate in aqueous or carbonic fluid is rapid at all temperatures and time scales of interest). Partial recrystallization during multiple pre-peak homogeneous or heterogeneous metamorphic reactions can result in cumulative clumped or bulk isotope compositions that are mixtures of all the relict generations of a single phase. Because we focus on contact metamorphic marbles that exhibit coarse, equilibrated fabrics, we examine simplified models in which carbonates thermometers always achieve their equilibrium values when they first reach their peak metamorphic temperatures. Instances where this condition is not met may be identifiable in some cases, as discussed below. However, note that these predictions differ from expectations for unmetamorphosed or weakly metamorphosed rocks in the outermost parts of contact metamorphic aureoles.

Our examination of the stable isotope systematics of carbonates from the Notch Peak aureole will assume a default model consisting of four stages in the thermal history: 1) crystallization at peak conditions in response to a local thermal disturbance, driving all carbonates to internal equilibrium Δ_{47} values and heterogeneous equilibrium with respect to calcite–dolomite fractionations of O and C isotopes; 2) cooling from peak conditions to the ambient temperature of the country rock; 3) incubation at this ambient temperature; and 4) exhumation and cooling to surface temperatures (Fig. 2).

The behavior of the various stable isotope homogeneous and heterogeneous equilibria will be determined by the kinetics controlling intracrystalline stable isotope distributions and intercrystalline exchange, as well as the peak temperature of recrystallization, the background ambient temperature in the crust at the depth of interest, and the rates of initial cooling and subsequent exhumation. We examine three end-member scenarios that could apply to any one of the isotopic proxies of interest:

- Case-1: The peak temperature is below the intrinsic (diffusion-limited) apparent equilibrium blocking temperature. Following crystallization at the peak temperature, isotopic redistribution in response to cooling cannot occur, and the peak temperature is faithfully recorded. In the case of heterogeneous equilibrium, it is unlikely that both minerals recrystallized at the same temperature. However, the rocks we examine, the product phase (dolomite) is low in overall abundance and produced at the expense of some of a large reservoir of the reactant phase; as long as the product equilibrates with the reactant at the peak temperature, then this temperature should still be preserved.
- Case-2: The apparent equilibrium blocking temperature falls between the peak temperature and the ambient temperature. As the rock cools from peak conditions, isotopic redistribution freely and continuously re-equilibrates until the partial reordering zone (i.e., the region where reordering is sluggish enough that the actual Δ_{47} value will lag behind the equilibrium Δ_{47} value) is reached. The exact apparent equilibrium blocking temperature that is preserved

depends on the cooling rate through this temperature window and how close the ambient temperature is to the nominal apparent equilibrium blocking temperature.

- Case-3: The apparent equilibrium blocking temperature falls below both the peak and ambient temperatures. All features of the peak temperature and initial cooling path are lost due to re-equilibration at the ambient temperature. The final recorded temperature will depend on the exhumation rate; e.g., in the limiting case of exhumation that is rapid enough to effectively quench early in the exhumation path, the ambient temperature of the crust at the depth of initial contact metamorphism will be preserved.

Thus, the final recorded temperature (based on Δ_{47} values of calcite or dolomite, or calcite–dolomite fractionations) may be interpreted as a constraint on one or more elements of the thermal history, depending on the relationship between the apparent equilibrium blocking temperature and the temperatures and rates of various key processes.

An essential point that guides our further development of these principles below is that many carbonate rocks possess several independent isotope equilibria: i.e., a calcite–dolomite marble records a Δ_{47} value of calcite, a Δ_{47} value of dolomite, and two calcite–dolomite heterogeneous equilibria (one for carbon isotopes and one for oxygen isotopes). Since the apparent equilibrium blocking temperatures for two or more of these isotope exchange thermometers are different, analysis of one rock should permit reconstruction of several features of the thermal history. For instance, given what is understood about the

reordering kinetics of these thermometers, for a metamorphic event with a peak temperature in excess of 300 °C and an ambient temperature near or below 200 °C, a single rock containing calcite and dolomite could quantitatively constrain the peak conditions, cooling path, and incubation temperature (i.e., ambient temperature at the relevant depth in the crust) of the event (Fig. 2).

Finally, it is important to note that the diffusion-controlled processes considered in our idealized model outlined above may be altered by recrystallization and/or fluid—rock reaction at temperatures other than the peak temperature. Such processes often can be recognized and characterized through texturally resolved isotopic measurements.

3. GEOLOGIC OVERVIEW OF THE NOTCH PEAK AUREOLE: A NATURAL LABORATORY FOR CLUMPED ISOTOPE REORDERING PROCESSES

We examine the stable isotope systematics, including clumped isotope compositions, of marbles from the Notch Peak contact metamorphic aureole in western Utah. The Notch peak pluton (Jg in Fig. 3) is a Late Jurassic-aged (Rb-Sr isochron age = 145 ± 1.9 Ma; Nabelek et al., 1988) quartz monzonite that discordantly intrudes into middle and upper Cambrian limestones, flat-lying at the time of intrusion, in the central portion the House Range, Utah (Hover-Granath et al., 1983). The surface

exposure of the pluton is approximately 7x4 km in area, although the body is believed to have a laccolithic shape (i.e., it is wider in the subsurface; Hover-Granath et al., 1983). Exhumation by block faulting in the Miocene Epoch has created exceptional exposure of the intrusion and host rocks surrounding it: the pluton can be observed in contact with as much as 800 m of vertical sedimentary section, and individual beds of the relevant units can be traced up to 6 km away from the contact with the pluton (Hover-Granath et al., 1983). The regional dip of the host limestones and dolostones is roughly 10° to the southeast, although proximal to the intrusion the strata are domed away from it. The metamorphic aureole surrounding the pluton has a regular, simple geometry; highest-grade marbles are found closest to the contact, with progressively lower grades found by moving directly away from it.

Among the units that are intruded by the Notch Peak Stock are the Weeks (Clw in Fig. 3) and Orr Formations: Cambrian limestones with subequal and minor silty/siliciclastic components, respectively. Additional intruded formations below the Weeks, including the Marjum Formation (Cmp in Fig. 3), are not considered in this study. Based on reconstruction of the regional sedimentary strata, the section overlying the Orr Formation was 6.2–6.5 km thick at the time of intrusion (Hover-Granath et al., 1983). The Big Horse Limestone Member (Cob in Fig. 3) of the Orr Fm. is a ~220 m-thick cliff-forming unit and the focus of this study (Hintze and Davis, 2002; Powell, 1959). The unit is composed of six cycles of argillite and limestone, each tens of meters thick. Each argillite grades gradually into limestone, consistent with a shallowing-upward shelf platform

sequence (Hover-Granath et al., 1983). The boundary between the top of each limestone and overlying argillite, however, is sharp (Hover-Granath et al., 1983). Many beds contain peloids, the upper cycles of the member are fossiliferous, and the top of each cycle is capped by an algal-rich or oolitic layer (Hover-Granath et al., 1983).

Nominally unmetamorphosed limestones in the Big Horse Member are primarily skeletal grainstones, with partial replacement by rhombohedral dolomite, and detrital silicate phases. Millimeter-sized cracks infilled with secondary calcite are common. The first identifiable metamorphic reaction in Big Horse limestones produces talc and tremolite, at a map distance of ~1.8 km from the contact with the pluton (Hover-Granath et al., 1983). At 0.8 km from the contact, the next isograd marks the first appearance of talc-free assemblages with tremolite or diopside as the primary medium-grade metamorphic phase. The highest-grade marbles, less than 0.25 km from the contact, are forsterite-bearing. Throughout the metamorphic suite, calcite and dolomite coarsen and change fabric, from skeletal and cement to hornfelsic or granoblastic grains 300–600 μm across. Temperatures of all meta-limestones from calcite–dolomite Mg-solvus thermometry are between 400 and 525 °C (Hover-Granath et al., 1983). Apparent temperatures measured with this technique in unmetamorphosed samples >5 km from the pluton are highly variable between 180 and 290 °C, and have been previously interpreted to represent relict diagenetic or primary sedimentary compositions, which likely never attained calcite–dolomite heterogeneous equilibrium, and therefore cannot be used to constrain the peak temperatures of these rocks (Hover-Granath et al., 1983). Although not the focus of this

study, the argillite layers contain a complementary trend in metamorphic grade, albeit with different index minerals (Hover-Granath et al., 1983).

3.1 FLUID FLOW IN THE NOTCH PEAK AUREOLE

Because the metamorphic and thermal history of the Notch Peak contact metamorphic aureole is relatively well understood, considerable efforts have been undertaken to study its history of fluid flow and reaction sequence. Bulk $\delta^{18}O$ values for meta-limestones are approximately constant throughout the aureole ($\delta^{18}O_{VSMOW}$ ~20‰), while those of meta-argillite layers decrease from ~18‰ in unmetamorphosed samples towards values as low as 8‰ in high-grade samples (Nabelek et al., 1984). This observation has been cited as strong evidence for higher time-integrated water fluxes in argillite than in limestone layers, possibly facilitated by reaction-enhanced permeability due to the increased capacity of this lithology for reaction of carbonate with co-existing silicate (Cui et al., 2002; Nabelek, 2009; Nabelek et al., 1984). The highest-grade argillite layers (wollastonite-bearing assemblages) are highly variable in $\delta^{18}O$, even at similar distances from the contact with the pluton, suggesting channelized fluid flow, and/or variations in mixing ratios of isotopically distinct magmatic and/or meteoric fluids. These findings, and the results from 2-D numerical models of thermal and fluid evolution in the aureole, have been cited as evidence for down-temperature fluid flow with a dominantly vertical component (i.e., up and away from the laccolith, perpendicular to bedding) (Nabelek, 2007; 2002; Nabelek et al., 1992). Although it has been argued that the

distribution of whole-rock $\delta^{18}O$ within 500 m of the contact and the observed location of the diopside-in isograd are better explained by a model of up-temperature, horizontal fluid flow (Ferry and Dipple, 1992), such conclusions are inconsistent with the results of hydrodynamic models of fluid flux in metamorphic terranes (Ferry et al., 2013).

We focus on limestones and meta-limestones from a single cycle at the top of the Big Horse Limestone Member; here, uniform bulk $\delta^{18}O$ values are strong evidence that, regardless of direction, fluid flow was minimal, being concentrated into adjacent argillite beds and limestone horizons in immediate contact with them. We narrow our focus onto these rocks in order isolate the effects of lateral temperature variations on the clumped isotope systematics of contact metamorphic rocks, anticipating that in a subsequent study we will apply these insights to understanding the more complex meta-argillite layers, and differences in thermal history with depth in the vertical section.

4. SAMPLES AND METHODS

4.1 SAMPLES

We examine the stable isotope, including clumped isotope, systematics of 60 aliquots (representing various phases and textures) from seven rock samples (Tables 2, 3). All but one (10H-107) are from the same limestone bed near the top of the Big

Horse Limestone Member. The bed commonly outcrops as the top layer of a ~20 m cliff, and a distinctive ooid-rich layer marks its top. The mineral assemblages, textures, whole-rock stable isotope values, and Mg concentration in calcite for five of the seven samples were previously studied in (Hover-Granath et al., 1983; Hover, 1981; Nabelek et al., 1984), and are representative of the unit at all metamorphic grades (from 0.01 to 5.36 km from the pluton contact). Two additional samples were collected by us in October 2012 to extend sampling below the talc-in isograd.

All seven samples contain minor dolomite. Dolomite/calcite ratios were measured by powder X-ray diffraction. Specifically, the relative heights of the strongest calcite and dolomite peaks (at 2-theta positions of 29.5 and 30.9, respectively) were compared to those of physical mixtures of calcite and dolomite standards, mixed in known proportions. Dolomite contents were all between 1.8 and 9.7% by weight.

4.2 STEPPED PHOSPHORIC ACID DIGESTION

Clumped isotope analysis of carbonate is commonly performed by evolving CO_2 from bulk carbonate powder reacted with 104% phosphoric acid, either overnight at 25 °C in McCrea-style reaction vessels, or for less than an hour at 90 °C in a common acid bath (e.g., see methods of Passey et al., 2010). When these methods are applied to powdered samples containing both calcite and dolomite, the evolved CO_2 is a mixture from each of these components (though the room temperature

extraction may leave some dolomite unreacted). To separately determine the $\delta^{13}C$, $\delta^{18}O$, and Δ_{47} of coexisting calcite and dolomite, we used a stepped reaction procedure, modified from the methods of Al-Aasm et al. (1990) and Guo (2009). First, all samples were ground to a fine powder and sifted to <106 μm to ensure a uniform grain size distribution. To obtain an isolated calcite-derived CO_2 fraction, ~15 mg of powder was reacted with 10 mL of 104% phosphoric acid in a glass vacuum reaction vessel immersed in a water bath equilibrated at 25 °C. For two hours, CO_2 evolved from the reaction was continuously frozen in liquid N_2 (LN_2 hereafter) on an adjacent glass U-trap. This continuous freezing prevented a buildup of pressure in the reaction vessel headspace, which was observed to slow the reaction rate and keep evolved CO_2 in the acid solution. This CO_2 fraction was separated from co-condensing H_2O by cryogenic procedures, and was sealed in a Pyrex™ break-seal. Any CO_2 evolved after the two-hour mark was discarded. To obtain an isolated dolomite-derived CO_2 fraction, a mass of powder containing the equivalent of ~20 mg of dolomite (150 – 500 mg total powder for our samples) was reacted in a McCrea-style vessel with 10 mL of acid (McCrea, 1950). For the first 24 hours, the reaction, conducted at 25 °C, was left open to a vacuum line backed by a liquid N_2 trap and a rough pump so that all CO_2 evolved during this step was removed and effectively none remained dissolved in the acid. At the end of 24 hours, the tube was evacuated using a mercury diffusion pump to baseline (~$1x10^{-2}$ Pa), closed off, immersed in a water bath at 50 ˚C and allowed to continue reaction, evolving CO_2 for an additional 24 hours. All CO_2 produced during this second step was cryogenically purified and sealed in a Pyrex™ tube. Tests on standard

powders demonstrated that no isotopic exchange between CO_2 and other oxygen reservoirs occurs when CO_2 is allowed to remain in the reaction vessel headspace for 24 hours at 50 °C.

It is well-established that the reaction of solid carbonate with anhydrous phosphoric acid to release CO_2, imparts an oxygen isotope fractionation between reacting carbonate and produced CO_2 that is phase-specific and temperature-dependent (Kim and O'Neil, 1997; Rosenbaum and Sheppard, 1986; Sharma and Clayton, 1965; Swart et al., 1991; Walters et al., 1972). Raw $\delta^{18}O$ values of CO_2 evolved from calcite (at 25 °C) and dolomite (at 50 °C) were corrected using previously determined fractionation factors ($\alpha^{18O}_{CO2\text{–}mineral}$, where $\alpha^{18O}_{a\text{–}b} = {}^{18}R_a/{}^{18}R_b$, and ${}^{18}R_a = [{}^{18}O]/[{}^{16}O]$ in phase 'a') of 1.01025 (Swart et al., 1991) and 1.01038 (Rosenbaum and Sheppard, 1986), respectively. For digestion at 90 °C in an automated common acid bath system, we used fractionation factors of 1.00821 for calcite (Swart et al., 1991) and 1.00922 for dolomite (based on a 2nd-order polynomial interpolation of 25, 50, and 100 °C data of Rosenbaum and Sheppard, 1986).

Based on the yields of tests on pure end-member standards, it was determined that 90% of calcite is digested in the first two hours at 25 ˚C, 10% in the following twenty-two. No calcite remains undigested after 24 hours at 25 °C, provided one continuously removes the headspace CO_2. Less than 1% of dolomite reacts in the first two hours, 30% over the first 24 hours at 25 °C, and 70% in the following 24 hours at 50 °C. Because nearly all samples in this study have less than 5% dolomite, any potential contribution of dolomite to the CO_2 evolved from calcite during the first two hours is negligible. Nevertheless, the

small but measurable rate of dolomite reaction at 25 ˚C may be important for any future studies of rocks containing greater proportions of dolomite. The most significant source of potential experimental error introduced by this method is that each fraction we collect (i.e., nominally calcite or dolomite) contains only a portion of the CO_2 from that phase (the first ~90 % of the CO_2 from calcite and the last ~70 % of the CO_2 from dolomite).

The efficacy and accuracy of our stepped phosphoric acid digestion method was tested by applying it to known mixtures of calcite and dolomite standards with distinct, known $\delta^{13}C$, $\delta^{18}O$, and Δ_{47} values. After the appropriate oxygen isotope reaction fractionation corrections were applied (as described above), we observed small but significant (<0.4‰ for $\delta^{18}O$, <0.2‰ for $\delta^{13}C$) discrepancies between the bulk isotope values of CO_2 from calcite and dolomite obtained using the stepped digestion method and those obtained by conventional online and offline reactions of the pure phases in the same analytical session (Table EA5). We believe that these discrepancies are caused by kinetic fractionations during the phosphoric acid reaction that are expressed due to the incomplete retrieval of digested CO_2 in any one step. We corrected for this artifact, (i.e., to better reflect the values we would have observed if phosphoric acid digestion had been complete), based on the average $\delta^{13}C$ and $\delta^{18}O$ values of replicate measurements of mixtures of dolomite and calcite standards, using our stepped digestion procedure (Tables 1, EA5). Δ_{47} values from mixed calcite and dolomite standards subject to offline stepped digestion

procedure were indistinguishable within error from values for complete offline digestion of pure samples; therefore, no correction was applied to Δ_{47} values of calcite and dolomite measured using the stepped digestion procedure.

4.3 STABLE ISOTOPE ANALYSIS OF PRODUCT CO_2

$\delta^{13}C$, $\delta^{18}O$, and Δ_{47} values for CO_2 produced from both offline stepped digestion in phosphoric acid and online bulk digestion in a common acid bath held at 90 °C were obtained using a Thermo 253 IRMS at Caltech following the methods outlined in Huntington et al., (2009), Passey et al. (2010) and Dennis et al., (2011). In brief, CO_2 was purified from contaminants using automated ethanol–CO_2 ice (~–67 °C) and LN_2 baths, and an online prep-GC system with a Porapak-Q 120/80 mesh column held at –20 °C. CO_2 voltages were measured at masses 44, 45, 46, 47, 48, and 49 and compared to a reference tank from Oztech in automatic dual inlet mode. Mass spectrometric nonlinearities were corrected for by observation of the dependence of Δ_{47} on bulk δ^{47} for pure CO_2 equilibrated at 1000 °C. At least one secondary carbonate standard was measured daily. Carbonate Δ_{47} values were projected into the interlaboratory absolute reference frame (ARF) using a secondary transfer function determined by routine measurement of gases equilibrated at 1000°C and 25 °C (Dennis et al., 2011). Samples reacted online at 90 °C were corrected to the 25 °C–Δ_{47} scale using the acid fractionation factor of 0.092‰ (in the ARF). The Δ_{47} acid fractionation factor

for dolomite reacted at 50 °C was determined by comparing the values obtained by offline digestion of an in-house pure dolomite standard to the average value of that standard when reacted on-line at 90 ˚C (for the same measurement sessions) and with the 0.092‰ correction applied. Based on the average of 5 offline standard dolomite digestions, a 50 °C acid fractionation factor of 0.040‰ was used to correct all dolomite samples to the 25 °C scale (Table EA6). This value is nearly identical to that that predicted for calcite analyzed at 50 ˚C (Ghosh et al., 2006), and is in agreement, within uncertainty, with the 50 °C fractionation factor experimentally determined for a variety of carbonate phases, including dolomite, by Defliese et al. (2015). Our correction is 0.030‰ smaller than that determined for a variety of dolomites, including the same reference standard used by Defliese et al. (2015), by Murray et al. (2016). Given the agreement between the Δ_{47}-T relationships of dolomite and calcite measured in our lab using both the common acid bath technique at 90 °C and sealed vessels at 25 °C (c.f., Fig. 3 in Stolper and Eiler (2015)), it seems clear to us that the large discrepancy in phosphoric acid fractionation factor between calcite and dolomite observed by Murray et al. (2016) must not apply to our analytical setup.

The relationship between Δ_{47} and temperature has been the subject of several studies, with some disagreement (e.g., Ghosh et al., 2006; Grauel et al., 2013; Kluge et al., 2015; Zaarur et al., 2013). The calibration is particularly poorly understood at high temperature, where calibration datasets are few, and small differences in Δ_{47} can amount to predicted temperature differences of many tens of degrees (Bonifacie et al., 2011; Kluge et al., 2015; Passey and Henkes, 2012, Stolper and Eiler,

2015). Much of the disagreement appears to result from interlaboratory methodological differences, possibly due to different acid digestion techniques or correction schemes for mass spectrometric artifacts (i.e., calibrations are generally coherent within labs but differ in temperature sensitivity between some labs). To minimize potential errors that interlaboratory discrepancies may introduce, we used a high-temperature calibration based on a dataset of synthetic calcites and dolomites grown at known temperatures and measured at Caltech on the same instrument as the data of this study: $\Delta_{47,ARF} = 0.001083 * \left({}^{10^6}/_{T^2}\right)^2 + 0.02854 * \left({}^{10^6}/_{T^2}\right) + 0.25865$, where T is in Kelvin. This is a second-order polynomial fit in Δ_{47} vs. $1/T^2$-space to the data of Ghosh et al. (2006), Guo et al. (2009), Boniface et al., (2011), and Stolper and Eiler (2015). Most of these data were generated before 25°C-equilibrated gases were routinely measured for correction to the absolute reference frame. Therefore, these data were projected into the absolute reference frame using a 1st-order linear least-squares fit (R^2 = 1.0) of accepted values of carbonate standards and 1000°C-equilibrated gases in the internal laboratory and absolute reference frames (i.e., the average secondary transfer function for this specific instrument; Dennis et al., 2011). We note that much of our interpretation of the following results rely on differences in Δ_{47} values (or lack thereof) among metamorphic grades and between phases, rather than the exact temperatures these values suggest.

5. RESULTS

We made a total of 32 measurements of calcite or dolomite extractions from seven samples using the offline stepped digestion technique. We also made 28 measurements of mixed samples of calcite and dolomite using the online common acid bath technique. The exact proportion of each carbonate phase was determined in each sample using the yields of calcite and dolomite from offline extractions, assuming that only 90% of all calcite present is reacted in the first step and 70% of all dolomite in the second (see Section 4.2 for details on how these yields, and associated corrections for the resulting fractionation, were determined). Calcite $\delta^{13}C$, $\delta^{18}O$, and Δ_{47} values for each online, common acid bath analysis were then determined by subtracting out the contribution of each of these values from the offline dolomite measurements of that sample, assuming calcite and dolomite contribute to the online common acid bath measurement in their measured proportions. Obviously this method could potentially introduce further errors because of some variability in the yields of carbonate phases during the partial digestions and uncertainty in the bulk isotope correction factors associated with these reactions. Moreover, errors in the calcite composition from each online measurement would be slightly correlated with errors in dolomite $\delta^{13}C$, $\delta^{18}O$, and Δ_{47} because the dolomite composition must be subtracted out. However, because dolomite is less than 10% (modal) of all samples, and in most cases less than 5%, these corrections were small (< 0.01‰ for Δ_{47}, which is less than the 1σ error of measurement), and any correlation would be undetectable. Because stable isotope indices have non-linear dependence on

proportions of end members in mixtures, these mixing calculations were made using concentrations of individual isotopologues and then converted to δ or Δ_{47} values. All 60 raw analyses are shown in Supplementary Tables 1, 2, and 3. Mean Δ_{47} values for each phase in each sample were obtained by calculating an error-weighted average of all replicates (n=2–9) using the equation $\left.\sum_{i=1}^{n} \frac{1}{{\sigma_i}^2} \Delta_{47,i} \right/ \sum_{i=1}^{n} \frac{1}{{\sigma_i}^2}$, where σ_i is the analytical standard error of each measurement. Reported uncertainty of each weighted mean is the standard deviation of all replicates divided by $\sqrt{n}$, where n is the number or replicates. The mean δ^{13}C, δ^{18}O, and weighted mean Δ_{47} values for each phase in each sample are reported in Tables 2 and 3.

Bulk δ^{13}C and δ^{18}O values from this study agree with published isotopic measurements of the same samples to within 0.27‰ (Nabelek et al., 1984; Table 2). Values of δ^{13}C and δ^{18}O for calcite are relatively constant at all distances in the aureole (Table 2). Calcite δ^{18}O (VPDB) ranges between –10.5 and –9.7‰, with no relation between oxygen isotopic composition and metamorphic grade. Except for sample 10H-107, which was taken from a different bed in the Big Horse Limestone Member than the other seven, all calcite δ^{13}C (VPDB) values fall between 0.6 and 1.0‰, again with no apparent trend with metamorphic grade. The slight variation in bulk δ^{13}C and δ^{18}O between beds in the unit is consistent with previous studies of the unit (Nabelek et al., 1984). Dolomite δ^{13}C and δ^{18}O values are heavier than the respective values for calcite at the same

location, by between 0.4 and 2‰ (Fig. 4). In general, dolomite $\delta^{13}C$ and $\delta^{18}O$ decrease with increasing metamorphic grade (Table 2).

Dolomite Δ_{47} values are roughly bimodal (Table 3). All samples within 2 km of the contact between limestone and pluton have Δ_{47} values between 0.340 and 0.360‰ (statistically indistinguishable from one another, within error). In contrast, dolomite in the three samples further than 2 km from the contact have Δ_{47} values ranging between 0.402 and 0.458. Calcite Δ_{47} values are all between 0.426 and 0.467‰, with no apparent trend vs. distance from the contact. All calcite Δ_{47} values are statistically indistinguishable from each other, within the errors on each set of replicate measurements (Fig. 5).

6. DISCUSSION

6.1 $\delta^{13}C$ AND $\delta^{18}O$ THERMOMETRY OF THE NOTCH PEAK AUREOLE

Values of $\delta^{13}C$ and $\delta^{18}O$ in calcite generally vary little (<0.9‰) between individual hand samples, with no systematic changes with distance from the pluton. The one exception, sample 10H-107, is from a different bed than the other seven samples, ~100 m lower in the Big Horse Limestone Member, and prior study of the formation suggests that this is likely just a reflection of original stratigraphic variations (Nabelek et al., 1984). Dolomite $\delta^{13}C$ and $\delta^{18}O$ values, on the other hand, decrease

by as much as much as 2.1 and 1.4‰, respectively, from unmetamorphosed limestones to Fo-bearing marbles. Because whole-rock isotopic composition can vary subtly among rocks from the same stratigraphic unit, we focus on the carbon-13 and oxygen-18 fractionation between coexisting calcite and dolomite in order to study the isotopic effects due solely to metamorphic reactions. We find a positive correlation between $\alpha^{13C}_{dol-cal}$ ($\alpha^{13C}_{dol-cal} = {}^{13}R_{dolomite}/{}^{13}R_{calcite}$, where ${}^{13}R_{mineral} = [{}^{13}C]/[{}^{12}C]$ in a given mineral) and distance to the pluton (Fig. 4). Similar behavior is suggested in oxygen isotope partitioning, but cannot be resolved in the high-grade samples outside of uncertainty (Fig. 4). All samples are rock-buffered, have no evidence of metasomatism, and have small dolomite/calcite ratios. As a result, the observed fractionations are largely controlled by the isotopic composition of dolomite in each sample. At least three processes can alter dolomite $\delta^{13}C$ and $\delta^{18}O$ values: decarbonation reactions, new dolomite growth during prograde metamorphism, and low temperature exchange with a hydrothermal fluid, either before metamorphism (i.e., diagenesis) or after. Dolomite recrystallization by grain coarsening also occurs during metamorphic events; this process modifies Δ_{47}, but should not alter $\delta^{13}C$ and $\delta^{18}O$ values unless it occurs in the presence of another phase that is exchangeable at the conditions of grain coarsening. It is likely that all three of these processes affected the studied samples to some extent, so the observed signal should not be attributed to exclusively one cause. Nevertheless, it is worth considering which is the primary control on the isotopic composition of dolomite across a metamorphic gradient, as this constrains the source and timing of dolomite formation in these samples.

Low-temperature alteration: one possible explanation of our findings is that dolomite in all samples was produced by infiltration of an Mg-bearing fluid during epigenesis prior to, or low-temperature recrystallization subsequent to, contact metamorphism. Indeed, this process must have occurred to produce dolomite in sample 12H-122, which was >5 km from the pluton contact and fully insulated from the metamorphic event. If this were true for all samples, the $\delta^{13}C$ and $\delta^{18}O$ values of dolomite in this case might be expected to be influenced both by host calcite and the dolomitizing fluid, and likely out of equilibrium with calcite. Given that calcite $\delta^{13}C$ does not correlate with distance or metamorphic grade, the trend between dolomite–calcite $\delta^{13}C$ fractionation and grade would thus be entirely coincidental.

This interpretation also is not supported by the textures of these samples. Diagenetic dolomite in sample 12H-122 (unmetamorphosed) occurs as fine-grained (~50–400 μm) rhombs replacing calcite in echinoids and peloids (Hover, 1981). In Fo-bearing high-grade marbles, however, coarse-grained (300–600 μm) dolomite has a granoblastic texture (Hover, 1981). Dolomite is a minor, scattered phase in the Big Horse Limestone Member, so the textural contrast between these rocks cannot be explained by grain coarsening alone. Rather, it suggests that while diagenetic dolomite was initially present in the bed, this was lost in contact metamorphosed samples, probably due to both dolomite-consuming reactions and high-temperature growth and grain coarsening. Thus, it seems reasonable to expect that $\delta^{13}C$ values were set during metamorphism, and there is no obvious evidence for retrograde or diagenetic modification of dolomite subsequent to metamorphism.

Calcite–dolomite stable isotope equilibrium: A second possibility is that trends in the $\delta^{13}C$ and $\delta^{18}O$ values of dolomite represent equilibrium inter-mineral fractionations between dolomite and calcite, which are established during dolomite growth at or near peak metamorphic conditions. Because the peak temperatures at all grades in the Notch Peak aureole are at or below the apparent equilibrium blocking temperatures for intercrystalline oxygen and carbon isotope diffusion in a quickly-cooled contact aureole (~600–800 °C, dependent on grain size, cooling rate, and f_{H2O}, Fig. 1), we expect the intermineral isotope thermometers to behave as case-1, above; i.e., they should faithfully record the temperature of equilibrium mineral crystallization (Sec. 2.2). We tested this prediction by comparing the temperatures given by these fractionations to peak temperatures in the unit at different distances, as calculated by published thermal models of the Notch Peak aureole (which are themselves made to be consistent with the phase equilibria determinations from the contact aureole). For this analysis, the empirical calibration of carbon-13 dolomite-calcite partitioning of Sheppard and Schwarcz (1970) and the experimentally-derived oxygen-18 calibration of Horita (2014) were used. The temperature profiles of Ferry and Dipple (1992) and Labotka et al. (1988) were used to estimate peak temperatures at all distances in the aureole. Following the convention of previous workers, reported distances are map distances to the pluton contact; true distances are smaller because the contact with the laccolithic pluton dips below the carbonate sequence (Labotka et al., 1988). Even so, given its position in the exposed, intruded section (>0.5 km above the base, Fig. 3), this discrepancy is likely insignificant.

With the exception of low-grade sample 20H-99, carbon-13-based temperatures largely agree with modeled peak temperatures within 3 km of the contact (Fig. 4). There is good reason to question the robustness of this finding: this temperature proxy is insensitive in this temperature range, and thus has particularly large errors in the highest-grade samples. Even so, the positive trend between dolomite–calcite carbon-13 fractionation and distance to the contact (i.e., smallest fractionations closest to the pluton) agrees with expectations, suggesting a dependence on peak temperature has been resolved. If this is the case, the anomalously large fractionation in sample 20H-99 may indicate that dolomite last crystallized from calcite during metamorphism somewhat below peak conditions in the sample. Large uncertainties in $\delta^{18}O$ fractionations obscure any trends within the metamorphosed samples. Even so, all metamorphosed samples have lower calcite–dolomite fractionations of $\delta^{18}O$ values than the most distal unmetamorphosed samples.

We consider it possible that some of the variation in C and O isotope distributions among carbonate phases reflects not only analytical errors but also disturbance of high temperature equilibrium by post-metamorphic isotopic redistributions. For instance, retrograde exsolution of dolomite from high-Mg calcite during cooling is a well-documented phenomenon; this can affect the accuracy of both bulk isotope fractionations (Wada and Suzuki, 1983), and the calcite–dolomite Mg-solvus thermometer (Müller et al., 2008). Indeed, fine exsolution lamellae of dolomite within calcite have been observed in the highest-grade sample in this study (10H-107; Hover-Granath et al., 1983), which may explain some scatter — assuming our

offline stepped digestion measurements succeeded at separating dolomite lamellae from host calcite. We also have not characterized the degree of grain-scale heterogeneity in stable isotope ratios of our samples, although it likely exists at some level (Ferry et al., 2010). Nevertheless, calcite–dolomite oxygen and carbon isotope fractionations are generally consistent with dolomite growth at or near peak temperatures in these samples. In the forsterite-bearing samples, the likely cause of this growth is the quartz-absent, tremolite-forming reaction: talc + calcite = tremolite + dolomite + H_2O + CO_2 (Hover-Granath et al., 1983).

Outside the talc + tremolite-in isograd, the correlations between calcite–dolomite stable isotope fractionations and distance are more robust. This is somewhat surprising given that the rhombohedral dolomite replacing carbonate clasts was previously interpreted to have a uniformly diagenetic origin in samples 12H-122 and 11H-116 (Hover, 1981). If these decreasing fractionations do represent dolomite crystallization at increasing temperatures, it would suggest that prograde dolomite growth from reaction of calcite occurred at anchimetamorphic conditions (i.e., below ~350 °C but above the ambient burial temperature of the unit) by a reaction that did not involve silicate phases.

Decarbonation reactions: At 150 MPa and moderate X_{CO_2} values, talc, tremolite, diopside, and forsterite are produced by decarbonation reactions involving dolomite and a silicate phase (c.f. Fig. 7 in Müller et al., 2008; Nabelek, 2002). The presence of these Mg-bearing silicate phases in the metamorphosed samples of the present study indicates that some amount of

decarbonation must have occurred. The CO_2–dolomite equilibrium oxygen isotope fractionation varies between ~5 and 7‰ at the temperatures of metamorphism in the Notch Peak aureole (O'Neil and Epstein, 1966), so it is conceivable that decarbonation could drive residual dolomite to lower $\delta^{18}O$ (Bottinga, 1968; Shieh and Taylor, 1969; Taylor and O'Neil, 1977; Wada and Suzuki, 1983). For example, the observed $\delta^{18}O$ of dolomite in the highest grade Notch Peak marbles can be explained by a model that assumes a starting $\delta^{18}O_{PDB}$ of –8.6‰ (equivalent to the dolomite in unmetamorphosed sample 12H-122), a CO_2–dolomite fractionation (α^{180}) given by: $1000\ln(\alpha^{180})=5$ (the approximate equilibrium CO_2–dolomite fractionation at 600 ˚C (Chacko and Deines, 2008; O'Neil and Epstein, 1966; it is less clear what should happen if the fractionation is kinetically controlled), and ~25% progress of dolomite decarbonation following the Rayleigh fractionation law ($^{18}R = {}^{18}R_0F^{\alpha-1}$, where F is the fraction of material remaining, ^{18}R is the oxygen isotope ratio of the remaining material, and $^{18}R_0$ is the initial ratio). This calculation assumes that the oxygen-bearing products of dolomite decarbonation do not exchange with the residue once generated, which is valid because temperatures throughout the aureole are too low for C or O-isotope exchange between dolomite and coexisting phases unless exchange is facilitated by recrystallization (e.g., Bergfeld et al., 2003). The carbon isotope effect of dolomite decarbonation has not been measured directly, but it can be estimated by dividing the CO_2–calcite carbon-13 fractionation by the equilibrium dolomite–calcite carbon-13 fractionation: $1000\ln(\alpha^{13C}_{CO2-dol}) \approx 3$ at 400–600 °C (Bottinga, 1968; Bottinga, 1969; Sheppard and Schwarcz, 1970; Nabelek, 1991; Chacko et al., 1991). Again, using this

fractionation and an initial $\delta^{13}C$ of 2.4‰ (the carbon isotopic composition of dolomite in sample 12H-122), the $\delta^{13}C$ of dolomite in the highest-grade samples can be generated with ~35% decarbonation.

The question is, are the effects of decarbonation recorded by dolomite, or were those effects erased by equilibration of dolomite with co-existing phases through grain coarsening or other mechanisms? Decarbonation seems likely to be the primary control of stable isotope variations only in samples that preserve textures consistent with dolomite-consuming reactions. Dolomite in the highly metamorphosed samples we examined is generally coarse-grained and granoblastic, suggesting grain growth rather than loss by decarbonation. We conclude that some dolomite decarbonation must have occurred near peak metamorphic conditions in order to produce forsterite, but that dolomite fabrics suggest any resulting stable isotope effects of this reaction are unlikely to have been preserved. It is also worth noting that this reaction is inferred to have consumed only a minor amount of the dolomite present (Hover-Granath et al., 1983).

Low-grade sample 20H-99, on the other hand, has strong textural evidence for dolomite decarbonation by the reaction: dolomite + quartz + H_2O➔calcite + talc + CO_2 (Hover-Granath et al., 1983). The sample contains talc and 2nd-generation, coarse-grained, hornfelsic calcite. Dolomite has a sub- to anhedral habit, unlike in more distal samples where it is rhombohedral (Hover, 1981). Despite the availability of bulk rock chemistry for the sample (Hover, 1981), the extent of dolomite decarbonation cannot be calculated directly without knowledge of the initial molar amounts of dolomite, quartz,

feldspars, and clay minerals. However, using the isotopic composition of dolomite in sample 12H-122 as an initial value, Rayleigh models for $\delta^{13}C$ and $\delta^{18}O$ predict reaction progress of ~25% and ~10%, respectively (see above for calculation details). The disagreement between the two isotope systems could have many causes, including incorrect starting compositions due to natural bulk rock variation (Table 2), inaccurate isotope fractionation factors for the decarbonation process, and isotopic zoning at the grain reaction front that was not measured in this study. Given these uncertainties, we simply conclude that the observed isotopic variation is consistent with such a mechanism.

All samples more than 1.6 km from the pluton contact are nominally unmetamorphosed (i.e., not talc-bearing), yet have resolvable differences in their dolomite–calcite isotopic fractionations that increase with distance. These samples cannot have undergone the lowest-temperature metamorphic decarbonation reaction observed in sample 20H-99, and we are not aware of any other decarbonation reaction that plausibly could have influenced their dolomite stable isotope compositions.

In summary, isotopic fractionations and textures in high-grade samples are most consistent with prograde dolomite growth in apparent equilibrium with calcite, even though some decarbonation and retrograde exsolution must have occurred. Dolomite in nominally unmetamorphosed samples was previously determined to be of diagenetic origin, but the trend in isotopic fractionations requires that dolomite growth occurred under anchimetamorphic conditions, when the local temperature was elevated due to the presence of the pluton (though no other metamorphic minerals were produced). The

texture and isotopic composition of dolomite in the low-grade talc-bearing sample are consistent with decarbonation of an originally-diagenetic endmember, although if dolomite in more distal samples has a metamorphic origin, it is possible that it does in sample 20H-99 as well.

6.2 DOLOMITE Δ_{47} VALUES

Much of the uncertainty in the preceding section regarding the origin of dolomite in the Notch Peak aureole can be addressed by considering the constraint imposed by dolomite Δ_{47} measurements. Unlike $\delta^{13}C$ and $\delta^{18}O$ values, dolomite Δ_{47} values can be reset by several mechanisms (solid state diffusion, heterogeneous reaction, and grain coarsening recrystallization), they are independent of bulk rock isotopic composition, and can be measured at a precision that is useful for comparison with independent determinations of peak metamorphic temperatures.

Apparent equilibrium blocking temperatures in high-grade marbles: Based on the arguments and data presented in section 2, we expect that the Δ_{47} value of dolomite in and near the Notch Peak aureole will have an apparent equilibrium blocking temperature above the ambient temperature (i.e., the crustal temperature far from the pluton) but below the peak temperature in the metamorphic aureole, and thus that it will behave as our case-2 geothermometer. We observe that the Δ_{47}

values of dolomites are indistinguishable in all samples inside the talc + tremolite-in isograd, with a weighted mean value that implies an apparent temperature of 328^{+13}_{-12} °C (1σ std error) (Fig. 5). This result closely resembles other measurements of dolomite marbles, which have been interpreted as apparent equilibrium blocking temperatures limited by intracrystalline atomic mobility (Ferry et al., 2011; Table S4). Therefore, we interpret the Δ_{47} values of dolomite inside the talc + tremolite-in isograd as the apparent equilibrium blocking temperatures of atomic re-arrangements during cooling from peak metamorphic temperatures. We cannot assess the effects of dolomite decarbonation or exsolution from calcite on Δ_{47} values because any such effect that occurred above the apparent equilibrium blocking temperature would have been obscured by solid state reordering during cooling. In fact, the uniform temperature of ~330 °C from dolomite Δ_{47} in all metamorphosed samples confirms that no retrograde dolomite modification occurred below this temperature.

This result is unsurprising given other studies of exsolution and retrograde isotopic exchange in calc-silicate contact metamorphic rocks. Metamorphism of such rocks is generally brief and drives off volatiles, lowering reaction rates; therefore, pervasive retrograde recrystallization long after peak conditions is rare (Cathles et al., 1997; Cook et al., 1997). For instance, in the Alta aureole in northern Utah, homogeneous calcite $\delta^{18}O$ and low calcite–dolomite X_{Mg} temperatures have been argued to indicate that carbonate recrystallization occurred, but only down to the temperature range of 500–550 °C, which is ~50 °C below peak conditions (Bowman et al., 2008; Cook et al., 1997; Cook and Bowman, 1994). When late-stage recrystallization,

exsolution, or isotopic exchange does occur, it is often because of exceptional conditions, such as multiple intrusive events, that produce polymetamorphism or a prolonged elevated temperature (e.g., Bowman et al., 2008; Lackey and Valley, 2004). For these reasons, we think that the conditions of metamorphism in marbles in the Big Horse Limestone member (dry, short-lived), and the preservation of near-equilibrium calcite–dolomite isotopic fractionations, support our interpretation that dolomite Δ_{47} values were set by intracrystalline isotopic redistribution rather than exsolution or some other heterogeneous reaction.

Peak temperatures in the outer aureole: The Ferry and Dipple (1992) and Nabelek et al., (1986) thermal models of the Notch Peak aureole suggest that a peak temperature of 330 °C occurs at a map distance of ~1.7 km from the contact with the pluton. In samples beyond this distance, dolomite should behave as a normal case-1 geothermometer and faithfully record the temperature of dolomite crystallization — i.e., either a diagenetic or burial metamorphic temperature, or perhaps a temperature corresponding to the peak reached by the cool, outer portions of the aureole (if that thermal pulse was associated with dolomite crystallization). Beginning with sample 11H-116 at a distance from the pluton of 1.9 km, we observe a trend of decreasing dolomite $T_{\Delta47}$ with increasing distance from the pluton that is largely consistent with thermal models of peak temperatures in the outer parts of the Notch Peak aureole (excluding sample 12-NPK-11b, see below), terminating with a value indistinguishable from the estimated background temperature (i.e., outside of any influence from the pluton) at 5.4 km

map distance to the contact. This is strong evidence for dolomite crystallization in response to heating from the intrusion. Moreover, the complementary lowering of dolomite $\delta^{13}C$ and $\delta^{18}O$ values suggests that this was not just recrystallization of diagenetic dolomite. Instead, it is likely that some dolomite crystallized through exchange with a local, rock-buffered fluid, such that the higher-temperature anchimetamorphic sample (11H-116) inherited a $\delta^{13}C$ and $\delta^{18}O$ composition closer to coexisting calcite than a lower-temperature sample (12-NPK-5) further from the intrusion. To our knowledge, this is the first time the thermal structure of a sub-greenschist grade metamorphic belt has been mapped with clumped isotopes. The variations in peak temperature recorded by Δ_{47} values of dolomite in this part of the aureole are otherwise cryptic; i.e., they are not documented by evidence preserved by mineral phase assemblages or textures.

Sample 12-NPK-11b is an exception to the pattern of dolomite Δ_{47} values described above. In this rock, abundant cm-scale cross-cutting secondary carbonate veining, and agreement between dolomite and calcite Δ_{47} thermometers, suggest that dolomite (along with calcite, see below) grew or recrystallized long after cooling from the peak temperatures reached in response to nearby intrusion, and prior to exhumation in the Miocene Epoch. We have omitted this sample from our discussion of peak metamorphism and cooling, as it seems obvious to us that it has been subject to a secondary process that disturbed the clumped isotope systematics. Curiously, the $\delta^{13}C$ and $\delta^{18}O$ fractionations between dolomite and calcite are still

consistent with the predicted peak temperature reached by the sample, implying that recrystallization of dolomite occurred in a rock-buffered system.

6.3 CALCITE Δ_{47} TEMPERATURES

Calcite Δ_{47} values are indistinguishable from each other, with an error-weighted mean of 0.446 ± 0.012 (2σ std. errors), which corresponds to an apparent temperature of 156 ± 12 °C. This temperature is generally consistent with the expected ambient temperature in the system far from the intrusion, given 6.2–6.5 km of overburden at the time of intrusion and a typical continental upper-crustal geotherm. However, two observations make this result unexpected: the apparent equilibrium temperature everywhere in the aureole, including its strongly metamorphosed inner regions, is modestly but significantly less than the apparent equilibrium blocking temperatures expected for slowly cooled calcite or observed apparent temperatures in common regional metamorphic marbles (Eiler, 2011; Henkes et al., 2014; Passey and Henkes, 2012; Stolper and Eiler, 2015). Also, calcite was expected to exhibit a case-2 thermometer behavior, like dolomite (Fig. 1). However, calcite apparent temperatures are statistically uniform across our sample suite, with no gradient with increasing distance from the pluton

contact. We show below that these two observations place significant new constraints on the geotherm and exhumation history of the crustal section intruded by the Notch Peak pluton.

Before we develop a thermal model based on these data, it is worth considering whether uniform calcite Δ_{47} values simply represent the temperature of some broad recrystallization event rather than a diffusion-limited, intracrystalline reordering process. The petrographic evidence does not support the former interpretation. Calcite grain size coarsens with metamorphic grade, and the ~300–600 μm, granoblastic textures in the highest-grade marble are unmistakably distinct from the finer-grained carbonate clasts with relict sedimentary textures in samples below but near the talc + tremolite-in isograd (Hover-Granath et al., 1983). If all samples were partially or completely recrystallized, these textural distinctions would be obscured. For this reason, we suggest that the uniform calcite Δ_{47} temperature of 156 ± 12 °C reflects intracrystalline atomic mobility during the temperature–time history of the aureole after intrusion and metamorphism.

6.4 A THERMAL MODEL FOR CALCITE Δ_{47} REORDERING IN A CONTACT AUREOLE

We explore this possibility using a 2-D thermal model of the Notch Peak pluton and surrounding country rock. The geometry and numerical grid spacing of the model replicate that of Nabelek (2009) for the same pluton: the model was 20 km

wide by 8 km deep, with grid spacing at 50 m. It was initialized with a laccolithic pluton 6 km wide and up to 2 km tall at the center, with a uniform initial temperature of 900°C. Initial conditions in the host rock were determined by a geothermal gradient of 25 °C/km, beginning at 75 °C at 3 km depth. Values for densities and radiogenic heat production terms in the monzonite and limestone are given in Table 4. Because of the significant dependence of thermal diffusivity and heat capacity on temperature (Whittington et al., 2009), these parameters were recalculated at every node for every time step. A finite-difference scheme was used to solve the thermal diffusion equation, plus the radiogenic heat production, in each 50m x 50m square, in one-year steps. Initial tests on a simple 1-D heat pulse of a similar scale demonstrated that this finite difference model accurately reproduced the analytical solution to this system. We accounted for the latent heat of crystallization using an *apparent* heat capacity term for the cooling pluton: $c^*_{app} = c_{mag} + \frac{\Delta H}{\Delta T}$, where the latent heat of fusion (ΔH = 246.5 J/g) is added over the temperature interval of crystallization (900–600 °C), and the magmatic heat capacity (c_{mag}) is the average of the crystalline and liquid granitic heat capacities (at the appropriate temperature), weighted by the fraction of melt remaining, assuming a linear increase in the amount of crystallization with drop in temperature (Nabelek et al., 2012). This results in an *apparent* thermal diffusivity term, $\kappa^* = \frac{k}{\rho c^*}$, which increases the rate at which heat diffuses out of the pluton and into the limestone until the monzonite is fully crystallized at 600 °C (Nabelek et al., 2012).

Our model makes several simplifying assumptions: the latent heat is released evenly over the prescribed temperature range; we do not account for heat transport by advective/convective fluid flow; and we do not consider the dependence of density on temperature, the contrasting fluid histories of interbedded limestone and argillite layers, or the state changes accompanying metamorphism in the inner aureole. We argue, however, that this model is sufficient for our purposes because 1) the meta-limestone layers of the Big Horse Limestone Member demonstrably experienced relatively little magmatic fluid infiltration, and 2) calcite clumped isotope apparent equilibrium blocking temperatures are only sensitive to the T–t path in the realm of approximately 125–300 °C. It is not necessary to accurately capture the fluid-controlled and reaction-controlled heat distribution in the early stages of metamorphism because these mechanisms do not significantly affect the bulk heat content of the system, especially in the limestones during late-stage cooling, when these mechanisms are no longer active.

The thermal model was run for 10 Ma. The T–t paths (in 1 year increments) at the positions of the studied samples were recorded. To explore the conditions under which the metamorphic apparent equilibrium blocking temperature signal can be completely lost to post-metamorphic, diffusion-limited reordering, we predicted the change in calcite Δ_{47} throughout the Notch Peak cooling history using both the calcite clumped isotope exchange–diffusion reordering model of Stolper and Eiler (2015) and the first order reordering model of Passey and Henkes (2012). Because the former model requires a functional form of T(t) to simultaneously solve the ordinary differential equations for the exchange and diffusion kinetic

parameters, we fit our model T–t paths to a version of the asymptotic cooling function of Ghose and Ganguly (1982): $T = {a}/{(1 + \frac{t+b}{c})} + d$, where a represents the theoretical peak temperature at $t + b = 0$, b is the temporal offset term used to obtain the actual peak temperature at $t = 0$, c is the cooling timescale, and d is the ambient temperature of the system. We initialized the models such that at time t=0, calcite Δ_{47} was in equilibrium with the peak temperature of the system. This could be achieved either by crystallization of calcite at peak conditions, or rapid diffusion-limited reordering to peak (or near-peak) conditions during the first few thousands of years. In every sample within 3 km of the contact, calcite clumped isotope reordering is rapid enough at t=0 that this condition is easily met. The peak temperature in this zone is also well above that at which Henkes et al. (2014) observed the decay of a rapid reordering component, which they attribute to the annealing of transient defects in the calcite crystal lattice. Therefore, it is sufficient to use their first-order approximation model, which considers only equilibrium, intrinsic defects. Following the convention of these workers, we use the kinetic parameters for optical calcite, as this material is most similar to the marbles in our system (i.e., we used the model of Passey and Henkes (2012)). Preliminary runs of both reordering models demonstrated that calcite clumped isotopes remain in equilibrium with cooling temperatures until ~350 °C. Since samples within the metamorphic aureole have similar cooling paths at and below 350 °C, a uniform T-t function can be used to model calcite Δ_{47} reordering in all samples within the mineralogically-defined metamorphic aureole.

Calcite Δ_{47} apparent equilibrium temperatures at the end of these runs were independent of peak temperature, and insensitive to late-stage cooling timescale (within the constraints on this parameter suggested by our 2-D thermal model), so the only realistically modifiable parameter is the long-term incubation temperature of the limestone bed (i.e., the ambient temperature at this depth, far from the influence of the pluton). To examine the sensitivity of the calcite Δ_{47} reordering process to residence temperature, we varied the ambient temperature of the system between 130 and 170 °C, while keeping all other T(t) fit parameters constant (specifically, a = 1079 °C, b = 2.05 x 10^4 years, c = 1.84 x 10^4 years in above equation). Calcite Δ_{47} reordering models were run for 100 Ma. Based on the overlying stratigraphic section, it is suggested that the depth of the studied bed (and, as a result, the ambient temperature of it) remained constant from the time of intrusion (~145 Ma; Nabelek et al., 1988) until exhumation in the Miocene Epoch, allowing for at least 100 Ma of residence at the ambient temperature of the system for Δ_{47} reordering prior to quenching during exhumation (Hintze and Davis, 2002; Hover-Granath et al., 1983). Calcite Δ_{47} reordering models for a similar Paleozoic Era sedimentary section in southeastern Nevada by Shenton et al. (2015) demonstrate that Basin and Range exhumation does quench this thermometer.

The essential criterion for evaluating these models is: under which conditions does calcite Δ_{47} fully equilibrate with the long term residence temperature, thereby erasing the difference in Δ_{47} between high grade metamorphic calcite close to the pluton and diagenetic calcite far from it? The difference between calcite Δ_{47} temperature and ambient (i.e., equilibrium)

temperature as a function time was considered for a range of residence temperatures (Fig. 6A). With the Stolper and Eiler (2015) model, calcite Δ_{47} fully equilibrates with a residence temperature of 170 °C, but only if given a full 100 Ma to do so. At residence temperatures of 160 °C and below, calcite Δ_{47} approaches but does not reach equilibrium, whereby a difference between high grade and unmetamorphosed calcite Δ_{47} is preserved. These models suggest that the observation of uniform calcite Δ_{47} temperatures of 156 ± 12 °C (2σ std. errors) is only possible if the true residence temperature was at the upper end of this range. In the Passey and Henkes (2012) model, full re-equilibration occurs for all residence temperatures above 150 °C (Fig. 6A). Thus, using the kinetic parameters for optical calcite from Passey and Henkes (2012), our measurements are compatible with a large range of acceptable residence temperatures.

Both sets of kinetic parameters are derived from linear regressions of Arrhenius plots with considerable uncertainty, especially when extrapolated to the temperatures of interest for this study. To explore the sensitivity of these models to the exact rate constants used, we varied the activation energies and natural log of the frequency factors by adding or subtracting up to 1σ uncertainty from their mean values. It is not immediately apparent how to generate families of likely kinetic parameters by perturbing these values within their reported uncertainties because their covariance matrices are not reported. For the Passey and Henkes (2012) model, we assumed that the populations of possible values for the activation energy and natural log of the frequency factor are perfectly anti-correlated, so Ea and $\ln K_0$ were varied in conjunction by the same

proportion of their 1σ uncertainty. This approach minimizes the change in the rate constants at the temperatures of interest, and is the most conservative estimate of the actual uncertainty on the linear regression; the true 1σ uncertainty envelope of the rate constants is likely larger. For the Stolper and Eiler (2015) model, we varied the Arrhenian parameters for the diffusion of singletons in this same way, while leaving the rate constants for isotopic exchange among pairs unmodified. Because diffusion of singletons is the rate-limiting step at the temperatures of interest, we observed that reasonable modifications of the Arrhenian parameters for isotope exchange among pairs had no effect on the model results.

The calcite Δ_{47} temperatures at the end of our 100 Ma T-t path are extremely sensitive to the kinetic parameters chosen (Fig. 6B, 6C). For the same residence temperature, final calcite Δ_{47} can range from fully equilibrated in the μ - 1σ models (i.e., lower activation energy and frequency factor, and a higher rate constant at the temperature of interest), to as much as 65 °C above thermal equilibrium in the μ + 1σ models (i.e., extrapolation of higher activation energy and frequency factor leading to slower reordering below ~300 °C). These results hold for both models (Figs. 6B, 6C). Comparison with the measured calcite Δ_{47} temperature of the bed indicates that while most sets of likely kinetic parameters for the Passey and Henkes (2012) model are compatible with our measurements over a wide range of residence temperatures, only iterations of the Stopler and Eiler (2015) model at the lower end of the 1σ uncertainty envelopes on the activation energy and natural log of the frequency factor for diffusion of singletons can reproduce the observed result. In addition, the final difference between calcite apparent

equilibrium temperature and residence temperature is sensitive to the exact residence temperature of the system. Using our temperature calibration and the most likely calcite reordering models, a marble incubated at 150 °C should fully re-equilibrate on the measured timescale (i.e., behave as a case-3 thermometer), while a marble held at 140 °C will retain an apparent equilibrium temperature of 170 °C (case-2 behavior). This has the intriguing implication that along a vertical transect of high-grade marbles in a contact aureole one would expect to observe an inverted temperature profile: hottest apparent equilibrium temperatures at the shallowest depth due to incomplete re-equilibration, and colder apparent equilibrium temperatures with increasing structural depth (Figs. 6B, 6C). Our dataset does not have the geometry to speak to the existence of this peculiar feature, but perhaps future studies will.

Our model fit to the observed distribution of calcite Δ_{47} values offers new constraints on the geologic history of the region surrounding the Notch Peak aureole. Barring heating by additional burial under a late-Mesozoic or Cenozoic unit that has since been completely eroded at a previously-unrecognized unconformity, our models indicate that the Big Horse Limestone Member can't have been exhumed much before the Miocene Epoch, else the difference in Δ_{47} values that must have existed between high-grade and unmetamorphosed calcites at the peak of metamorphism would have been preserved. Moreover, assuming the estimate of overlying sediment thickness of 6.2–6.5 km from Hover-Granath et al. (1983) is correct, this result provides a tight constraint on the local geotherm; even when expanding the range of acceptable ambient

temperatures to 145–170 °C (to allow for some error on the Δ_{47}–temperature calibration), the Cenozoic upper crustal geotherm must have been between 22.3 and 27.4 °C/km. This range is typical for the shallow crust in passive continental interiors (Nathenson and Guffanti, 1988), but significantly lower than the modern borehole-derived thermal gradients in the area surrounding Notch Peak (greater than 30 °C/km, often much greater; Blackett, 2004). This observation is consistent with the transition to the Basin and Range extensional regime in the Miocene Epoch, where crustal thinning increased local heat flow and steepened thermal gradients. Accurate slopes and, especially, shapes of paleo-geothermal gradients, are essential in order to properly estimate denudation/erosion rates in low-temperature thermochronometric studies (e.g., Dempster and Persano, 2006). Although our 1-D study cannot constrain the shape of the paleo-geotherm, it demonstrates the potential of multiple-phase clumped isotope techniques to address such problems.

7. CONCLUSIONS

Even in rocks as simple as two-phase dolomite-bearing limestones, four stable isotope geothermometers are available to determine the thermal histories of metamorphic events. Because these four thermometers have different re-equilibration behaviors in response to changing conditions, they record distinct aspects of the cooling history of a sample, and collectively impose surprisingly nuanced constraints on temperature–time history. In the Notch Peak aureole, UT, $\alpha^{13C}{}_{dol-cal}$ and $\alpha^{18O}{}_{dol-cal}$ fractionations from coexisting calcite and dolomite correlate with distance to the intruded pluton, indicating relatively rapid

cooling and minimal modification subsequent to peak conditions. Within 4 km to the contact, temperatures in equilibrium with the $\alpha^{13C}_{dol-cal}$ fractionations largely agree with those expected from thermal models of the aureole, but large uncertainties on the measurements preclude their use as precise indicators of crystallization temperature. At greater distances, the disagreement between $\alpha^{13C}_{dol-cal}$ and $\alpha^{18O}_{dol-cal}$ fractionation temperatures is an indication of diagenetic dolomite growth out of isotopic equilibrium with coexisting calcite. Notably, this result implies that metamorphic recrystallization in response to the thermal pulse occurred in rocks beyond, but near, the talc + tremolite–in isograd and the nominal onset of metamorphism. Dolomite Δ_{47} values record apparent equilibrium blocking temperatures in the inner metamorphic aureole and peak temperatures in the outer aureole. The interface between the two maps the location of the ~330 °C isograd, and thus metamorphic grades below the onset of easily recognized greenschist-facies metamorphism can be distinguished. Calcite Δ_{47} values are constant across the entire range of studied samples, which requires complete reordering down to the ambient temperature of the system following the metamorphic event. We use multiple calcite Δ_{47} reordering models to show that not only is this behavior consistent with cooling history of the aureole, it constrains the exact incubation temperature of the unit throughout the late Mesozoic and Cenozoic Eras. Together, the two clumped isotope thermometers suggest that the unit was held at 145–170 °C for at least ~100 Ma until exhumation in the Miocene Epoch.

ACKNOWLEDGMENTS

We would like to thank Julita Penido for her assistance with sample collection, Daniel Stolper for his instruction in modeling solid-state calcite reordering, and Nami Kitchen and Kristin Bergmann for their assistance with analytical techniques. George Rossman provided an additional sample and helpful discussion that strengthened this paper. Theodore Labotka and two anonymous reviewers provided thoughtful suggestions that greatly improved the quality of this paper. This research was funded by the Petrology and Geochemistry Program of the United States National Science Foundation (EAR–1322058).

REFERENCES

Ahrens T. J. and Johnson M. L. (1995) Shock wave data for rocks. *Rock physics & phase relations: A handbook of physical constants*, 35–44.

Al-Aasm I. S., Taylor B. E. and South B. (1990) Stable isotope analysis of multiple carbonate samples using selective acid extraction. *Chemical Geology: Isotope Geoscience section* **80**, 119–125.

Anderson T. F. (1972) Self-diffusion of carbon and oxygen in dolomite. *J. Geophys. Res.* **77**, 857–862.

Bergfeld D., Nabelek P. I. and Labotka T. C. (2003) Carbon isotope exchange during polymetamorphism in the Panamint Mountains, California, USA. *Journal of Metamorphic Geology* **14**, 199–212.

Blackett R. E. (2004) Geothermal gradient data for Utah. *Geothermal Resources Council Transactions*.

Bonifacie M., Ferry J. M., Horita J., Vasconcelos C., Passey B. H. and Eiler J. M. (2011) Calibration and applications of the dolomite clumped isotope thermometer to high temperatures. *Mineralogical Magazine* **75**, 551.

Bottinga Y. (1969) Calculated fractionation factors for carbon and hydrogen isotope exchange in the system calcite-carbon dioxide-graphite-methane-hydrogen-water vapor. *Geochimica et Cosmochimica Acta* **33**, 49–64.

Bottinga Y. (1968) Calculation of fractionation factors for carbon and oxygen isotopic exchange in the system calcite-carbon dioxide-water. *J. Phys. Chem.* **72**, 800–808.

Bowman J. R., Valley J. W. and Kita N. T. (2008) Mechanisms of oxygen isotopic exchange and isotopic evolution of 18O/16O-depleted periclase zone marbles in the Alta aureole, Utah: insights from ion microprobe analysis of calcite. *Contrib Mineral Petrol* **157**, 77–93.

Bristow T. F., Bonifacie M., Derkowski A., Eiler J. M. and Grotzinger J. P. (2011) A hydrothermal origin for isotopically anomalous cap dolostone cements from south China. *Nature* **474**, 68–71.

Cathles L. M., Erendi A. H. J. and Barrie T. (1997) How long can a hydrothermal system be sustained by a single intrusive event? *Economic Geology* **92**, 766–771.

Chacko T. and Deines P. (2008) Theoretical calculation of oxygen isotope fractionation factors in carbonate systems. *Geochimica et Cosmochimica Acta* **72**, 3642–3660.

Chacko T., Mayeda T. K., Clayton R. N. and Goldsmith J. R. (1991) Oxygen and carbon isotope fractionations between CO 2 and calcite. *Geochimica et Cosmochimica Acta* **55**, 2867–2882.

Cook S. J. and Bowman J. R. (1994) Contact metamorphism surrounding the Alta stock; thermal constraints and evidence of advective heat transport from calcite+ dolomite geothermometry. *American Mineralogist* **79**, 513–525.

Cook S. J., Bowman J. R. and Forster C. B. (1997) Contact metamorphism surrounding the Alta stock: Finite element model simulation of heat- and 18O/16O mass-transport during prograde metamorphism. *American Journal of Science* **297**.

Cui X., Nabelek P. I. and Liu M. (2002) Numerical modeling of fluid flow and oxygen isotope exchange in the Notch Peak

contact-metamorphic aureole, Utah. *Geological Society of America Bulletin* **114**, 869–882.

Dale A., John C. M., Mozley P. S., Smalley P. C. and Muggeridge A. H. (2014) Time-capsure concretions: Unlocking burial diagaenetic processes in the Mancos Shale using carbonate clumped isotopes. *Earth and Planetary Science Letters* **394**, 30–37.

Defliese W. F., Hren M. T., and Lohmann K. C. (2015) Compositional and temperature effects of phosphoric acid fractionation on Δ_{47} analysis and implications for discrepant calibrations. *Chemical Geology* **396**, 51-60.

Deines P. (2004) Carbon isotope effects in carbonate systems. *Geochimica et Cosmochimica Acta* **68**, 2659–2679.

Dempster T. J. and Persano C. (2006) Low-temperature thermochronology: Resolving geotherm shapes or denudation histories? *Geology* **34**, 73–76.

Dennis K. J. and Schrag D. P. (2010) Clumped isotope thermometry of carbonatites as an indicator of diagenetic alteration. *Geochimica et Cosmochimica Acta* **74**, 4110–4122.

Dennis K. J., Affek H. P., Passey B. H., Schrag D. P. and Eiler J. M. (2011) Defining an absolute reference frame for "clumped" isotope studies of CO2. *Geochimica et Cosmochimica Acta* **75**, 7117–7131.

Dodson M. H. (1973) Closure temperature in cooling geochronological and petrological systems. *Contrib Mineral Petrol* **40**, 259–274.

Eiler J. M. (2011) Paleoclimate reconstruction using carbonate clumped isotope thermometry. *Quaternary Science Reviews* **30**, 3575–3588.

Eiler J. M. and Schauble E. (2004) 18O13C16O in Earth's atmosphere. *Geochimica et Cosmochimica Acta* **68**, 4767–4777.

Eiler J. M., Baumgartner L. P. and Valley J. W. (1992) Intercrystalline stable isotope diffusion: a fast grain boundary model. *Contrib Mineral Petrol* **112**, 543–557.

Epstein S., Buschsbaum R., Lowenstam H. A. and Urey H. C. (1953) Revised carbonate-water isotopic temperature scale.

Geological Society of America Bulletin **64**, 1315.

Farver J. R. (1994) Oxygen self-diffusion in calcite: Dependence on temperature and water fugacity. *Earth and Planetary Science Letters* **121**, 575–587.

Ferry J. M. and Dipple G. M. (1992) Models for coupled fluid flow, mineral reaction, and isotopic alteration during contact metamorphism: the Notch Peak aureole, Utah. *American Mineralogist* **77**, 577–591.

Ferry J. M., Wing B. A., Penniston-Dorland S. C. and Rumble D. (2002) The direction of fluid flow during contact metamorphism of siliceous carbonate rocks: new data for the Monzoni and Predazzo aureoles, northern Italy, and a global review. *Contributions to Mineralogy and Petrology* **142**, 679-699.

Ferry J. M., Passey B. H., Vasconcelos C. and Eiler J. M. (2011) Formation of dolomite at 40-80 C in the Latemar carbonate buildup, Dolomites, Italy, from clumped isotope thermometry. *Geology* **39**, 571–574.

Ferry J. M., Ushikubo T., Kita N. T. and Valley J. W. (2010) Assessment of grain-scale homogeneity and equilibration of carbon and oxygen isotope compositions of minerals in carbonate-bearing metamorphic rocks by ion microprobe. *Geochimica et Cosmochimica Acta* **74**, 6517–6540.

Ferry J. M., Winslow N. W. and Penniston-Dorland S. C. (2013) Re-evaluation of Infiltration-driven Regional Metamorphism in Northern New England: New Transport Models with Solid Solution and Cross-layer Equilibration of Fluid Composition. *Journal of Petrology* **54**, 2455–2485.

Frey M. (1987) Very low-grade metamorphism of clastic sedimentary rocks. In *Low temperature metamorphism* Blackie Glasgow. pp. 9–58.

Ghose S. and Ganguly J. (1982) Mg-Fe Order-Disorder in Ferromagnesian Silicates. In *Advances in Physical Geochemistry* (ed. S. Saxena). Advances in Physical Geochemistry. Springer New York, New York, NY. pp. 3–99–99.

Ghosh P., Adkins J., Affek H., Balta B., Guo W., Schauble E. A., Schrag D. and Eiler J. M. (2006) 13C–18O bonds in carbonate minerals: A new kind of paleothermometer. *Geochimica et Cosmochimica Acta* **70**, 1439–1456.

Grauel A.-L., Schmid T. W., Bin Hu, Bergami C., Capotondi L., Zhou L. and Bernasconi S. M. (2013) Calibration and application of the "clumped isotope" thermometer to foraminifera for high-resolution climatereconstructions. *Geochimica et Cosmochimica Acta* **108**, 125–140.

Guo W. (2009) Carbonate clumped isotope thermometry: application to carbonaceous chondrites and effects of kinetic isotope fractionation.

Guo W., Mosenfelder J. L., Goddard W. A. III and Eiler J. M. (2009) Isotopic fractionations associated with phosphoric acid digestion of carbonate minerals: Insights from first-principles theoretical modeling and clumped isotope measurements. *Geochimica et Cosmochimica Acta* **73**, 7203–7225.

Henkes G. A., Passey B. H., Grossman E. L., Shenton B. J., Pérez-Huerta A. and Yancey T. E. (2014) Temperature limits for preservation of primary calcite clumped isotope paleotemperatures. *Geochimica et Cosmochimica Acta* **139**, 362–382.

Hintze L. F. and Davis F. D. (2002) Geologic map of the Tule Valley 30'x 60' Quadrangle and parts of the Ely, Fish Springs, and Kern Mountains 30" x 60" Quadrangles, northwest Millard County, Utah. *Utah Geological Survey Map* **30**, 60.

Horita J. (2014) Oxygen and carbon isotope fractionation in the system dolomite–water–CO. *Geochimica et Cosmochimica Acta* **129**, 111–124.

Hover-Granath V. C., Papike J. J. and Labotka T. C. (1983) The Notch Peak contact metamorphic aureole, Utah: Petrology of the Big Horse limestone member of the Orr Formation. *Geological Society of America Bulletin* **94**, 889–906.

Hover V. C. (1981) The Notch Peak Metamorphic Aureole, Utah: Mineralogy, petrology, and geochemistry of the Big Horse Canyon member of the Orr formation. State University of New York at Stony Brook.

Humphrey F. L. and Wyatt M. (1958) Scheelite in feldspathized granodiorite at the Victory Mine, Gabbs, Nevada. *Economic Geology* **53**, 38-64.

Huntington K. W., Budd D. A., Wernicke B. P. and Eiler J. M. (2011) Use of Clumped-Isotope Thermometry To Constrain the Crystallization Temperature of Diagenetic Calcite. *Journal of Sedimentary Research* **81**, 656–669.

Huntington K. W., Eiler J. M., Affek H. P., Guo W., Bonifacie M., Yeung L. Y., Thiagarajan N., Passey B., Tripati A., Daëron M. and Came R. (2009) Methods and limitations of "clumped" CO 2isotope (Δ 47) analysis by gas-source isotope ratio mass spectrometry. *J. Mass Spectrom.* **44**, 1318–1329.

Kim S.-T. and O'Neil J. R. (1997) Equilibrium and nonequilibrium oxygen isotope effects in synthetic carbonates. *Geochimica et Cosmochimica Acta* **61**, 3461–3475.

Kirschner D. L., Sharp Z. D. and Masson H. (1995) Oxygen isotope thermometry of quartz-calcite veins: Unraveling the thermal-tectonic history of the subgreenschist facies Morcles nappe (Swiss Alps). *Geological Society of America Bulletin* **107**, 1145–1156.

Kluge T., John C. M., Jourdan A.-L., Davis S. and Crawshaw J. (2015) Laboratory calibration of the calcium carbonate clumped isotope thermometer in the 25–250°C temperature range. *Geochimica et Cosmochimica Acta* **157**, 213–227.

Labotka T. C., Cole D. R., Fayek M. J. and Chacko T. (2011) An experimental study of the diffusion of C and O in calcite in mixed CO2-H2O fluid. *American Mineralogist* **96**, 1262–1269.

Labotka T. C., Nabelek P. I. and Papike J. J. (1988) Fluid infiltration through the Big Horse Limestone Member in the Notch Peak contact-metamorphic aureole, Utah. *American Mineralogist* **73**, 1302–1324.

Lackey J. S. and Valley J. W. (2004) Complex patterns of fluid flow during wollastonite formation in calcareous sandstones at Laurel Mountain, Mt. Morrison Pendant, California. *Geological Society of America Bulletin* **116**, 76.

Lange R. A. (2003) The fusion curve of albite revisited and the compressibility of NaAlSi 3O 8liquid with pressure. *American Mineralogist* **88**, 109–120.

Lasaga A. C. (1998) *Kinetic Theory in the Earth Sciences*, Princeton University Press.

Lloyd M. K. and Eiler J. M. (2014) Laboratory and natural constraints on the temperature limit for preservation of the dolomite clumped isotope thermometer. *AGU Fall Meeting 2014*, Abstract #V11A-4694.

Matthews A. and Katz A. (1977) Oxygen isotope fractionation during the dolomitization of calcium carbonate. *Geochimica et*

Cosmochimica Acta **41**, 1431–1438.

McCrea J. M. (1950) On the Isotopic Chemistry of Carbonates and a Paleotemperature Scale. *J. Chem. Phys.* **18**, 849–857.

Mullis J., Dubessy J., Poty B. and O'Neil J. (1994) Fluid regimes during late stages of a continental collision: Physical, chemical, and stable isotope measurements of fluid inclusions in fissure quartz from a geotraverse through the Central Alps, Switzerland. *Geochimica et Cosmochimica Acta* **58**, 2239–2267.

Müller T., Baumgartner, L.P., Foster C. T. and Roselle G. T. (2008) Forward modeling of the effects of mixed volatile reaction, volume diffusion, and formation of submicroscopic exsolution lamellae on calcite-dolomite thermometry. *American Mineralogist* **93**, 1245–1259.

Murray S. T., Arienzo M. M., and Swart P. K. (2016) Determining the Δ_{47} acid fractionation in dolomites. *Geochimica et Cosmochimica Acta* **174**, 42-53.

Nabelek P. I. (2002) Calc-silicate reactions and bedding-controlled isotopic exchange in the Notch Peak aureole, Utah: implications for differential fluid fluxes with metamorphic grade. *Journal of Metamorphic Geology* **20**, 429–440.

Nabelek P. I. (2007) Fluid evolution and kinetics of metamorphic reactions in calc-silicate contact aureoles—From H2O to CO2 and back. *Geology* **35**, 927.

Nabelek P. I. (2009) Numerical Simulation of Kinetically-controlled calc-silicate reactions and fluid flow with fransie. *American Journal of Science* **309**, 517–548.

Nabelek P. I. (1991) Stable isotope monitors. *Reviews in Mineralogy and Geochemistry* **26**, 395–435.

Nabelek P. I., Hofmeister A. M. and Whittington A. G. (2012) The influence of temperature-dependent thermal diffusivity on the conductive cooling rates of plutons and temperature-time paths in contact aureoles. *Earth and Planetary Science Letters* **317–318 IS -**, 157–164.

Nabelek P. I., Labotka T. C., O'neil J. R. and Papike J. J. (1984) Contrasting fluid/rock interaction between the Notch Peak granitic intrusion and argillites and limestones in western Utah: Evidence from stable isotopes and phase assemblages.

Contrib Mineral Petrol **86**, 25–34.

Nabelek P. I., Papike J. J. and Laul J. C. (1986) The Notch Peak Granitic Stock, Utah: Origin of Reverse Zoning and Petrogenesis. *Journal of Petrology* **27**, 1035–1069.

Nabelek P., Hanson G., Labotka T. and Papike J. (1988) Effects of fluids on the interaction of granites with limestones: The Notch Peak stock, Utah. *Contrib Mineral Petrol* **99**, 49–61–61.

Nathenson M. and Guffanti M. (1988) Geothermal gradients in the conterminous United States. *J. Geophys. Res. Solid Earth* **93**, 6437–6450.

Nelson C. A. (1962) Lower Cambrian-Precambrian Succession, White-Inyo Mountains, California. *Geological Society of America Bulletin* **73**, 139–144.

O'Neil J. R. and Epstein S. (1966) Oxygen Isotope Fractionation in the System Dolomite-Calcite-Carbon Dioxide. *Science* **152**, 198–201.

Passey B. H. and Henkes G. A. (2012) Carbonate clumped isotope bond reordering and geospeedometry. *Earth and Planetary Science Letters* **351–352**, 223–236.

Passey B. H., Levin N. E., Cerling T. E., Brown F. H. and Eiler J. M. (2010) High-temperature environments of human evolution in East Africa based on bond ordering in paleosol carbonates. *Proceedings of the National Academy of Sciences* **107**, 11245–11249.

Powell D. K. (1959) The Geology of Southern House Range, Millard County, Utah. *UGS Files*, 1–56.

Rosenbaum J. and Sheppard S. M. F. (1986) An isotopic study of siderites, dolomites and ankerites at high temperatures. *Geochimica et Cosmochimica Acta* **50**, 1147–1150.

Rosenbaum J. M. (1994) Stable isotope fractionation between carbon dioxide and calcite at 900°C. *Geochimica et Cosmochimica Acta* **58**, 3747–3753.

Schauble E. A., Ghosh P. and Eiler J. M. (2006) Preferential formation of 13C–18O bonds in carbonate minerals, estimated using first-principles lattice dynamics. *Geochimica et Cosmochimica Acta* **70**, 2510–2529.

Sharma T. and Clayton R. N. (1965) Measurement of O18O16 ratios of total oxygen of carbonates. *Geochimica et Cosmochimica Acta* **29**, 1347–1353.

Shenton B. J., Grossman E. L., Passey B. H., Henkes G. A., Becker T. P., Laya J. C., Pérez-Huerta A., Becker S. P. and Lawson M. (2015) Clumped isotope thermometry in deeply buried sedimentary carbonates: The effects of bond reordering and recrystallization. *Geological Society of America Bulletin*.

Sheppard S. M. F. (1986) Characterization and isotopic variations in natural waters. *Reviews in Mineralogy and Geochemistry* **16**, 165–183.

Sheppard S. M. F. and Schwarcz H. P. (1970) Fractionation of carbon and oxygen isotopes and magnesium between coexisting metamorphic calcite and dolomite. *Contrib Mineral Petrol* **26**, 161–198.

Shieh Y. N. and Taylor H. P. Jr (1969) Oxygen and hydrogen isotope studies of contact metamorphism in the Santa Rosa Range, Nevada and other areas. *Contrib Mineral Petrol* **20**, 306–356.

Stolper D. A. and Eiler J. M. (2015) The kinetics of solid-state isotope-exchange reactions for clumped isotopes: A study of inorganic calcites and apatites from natural and experimental samples. *American Journal of Science* **315**, 363–411.

Swart P. K., Burns S. J. and Leder J. J. (1991) Fractionation of the stable isotopes of oxygen and carbon in carbon dioxide during the reaction of calcite with phosphoric acid as a function of temperature and technique. *Chemical Geology: Isotope Geoscience section* **86**, 89–96.

Talvitie N. A. (1951) Determination of Quartz in Presence of Silicates Using Phosphoric Acid. *Analytical Chemistry* **23**, 623–626.

Taylor B. E. and O'Neil J. R. (1977) Stable isotope studies of metasomatic Ca-Fe-Al-Si skarns and associated metamorphic and igneous rocks, Osgood Mountains, Nevada. *Contrib Mineral Petrol* **63**, 1–49.

Tenner T. J., Lange R. A. and Downs R. T. (2007) The albite fusion curve re-examined: New experiments and the high-pressure

density and compressibility of high albite and NaAlSi3O8 liquid. *American Mineralogist* **92**, 1573–1585.

Tool A. Q. (1946) Relation between inelastic deformability and thermal expansion of glass in its annealing range*. *J American Ceramic Society* **29**, 240–253.

Vitaliano C. J., Callaghan E. and Silberling N. J. (1957) *Geology of Gabbs and vicinity, Nye County, Nevada*, USGS.

Wada H. and Suzuki K. (1983) Carbon Isotopic Thermometry Calibrated by Dolomite-Calcite Solvus Temperatures. *Geochimica et Cosmochimica Acta* **47**, 697–706.

Walters L. J. Jr., Claypool G. E. and Choquette P. W. (1972) Reaction rates and $\delta^{18}O$ variation for the carbonate-phosphoric acid preparation method. *Geochimica et Cosmochimica Acta* **36**, 129–140.

Wang Z., Schauble E. A. and Eiler J. M. (2004) Equilibrium thermodynamics of multiply substituted isotopologues of molecular gases. *Geochimica et Cosmochimica Acta* **68**, 4779–4797.

Whittington A. G., Hofmeister A. M. and Nabelek P. I. (2009) Temperature-dependent thermal diffusivity of the Earth's crust and implications for magmatism. *Nature* **458**, 319–321.

Wollenberg H. A. and Smith A. M. (1987) Radiogenic Heat-Production of Crustal Rocks — an Assessment Based on Geochemical Data. *Geophys. Res. Lett.* **14**, 295–298.

Zaarur S., Affek H. P. and Brandon M. T. (2013) A revised calibration of the clumped isotope thermometer. *Earth and Planetary Science Letters* **382**, 47–57.

Zhang Y. (2010) Diffusion in Minerals and Melts: Theoretical Background. *Reviews in Mineralogy and Geochemistry* **72**, 5–59.

FIGURE CAPTIONS

Fig. 1: Apparent equilibrium blocking temperatures of single isotope and bulk isotope thermometers in calcite and dolomite. Carbon-13, and dry (X_{CO2} = 1) oxygen-18 lines are derived from the calcite diffusion experiments of Labotka et al. (2011). Wet oxygen-18 parameters are from the calcite data of Farver (1994). Following the convention of Labotka et al. (2011), all three single isotope exchange apparent equilibrium blocking temperature relations are calculated using the Dodson-style equation of Lasaga (1998), assuming linear cooling rates and a grain size of 100 μm: $T_c = \frac{E_a/R}{\ln[2K_0T_c^2/(a^2SE_a/R)]}$, where Ea, R, K_0, T_c, a, and S are the activation energy, gas constant, frequency factor, apparent equilibrium blocking temperature, grain radius, and cooling rate, respectively. These curves implicitly assume that self-diffusion in calcite is the rate-limiting step to re-equilibration, which is consistent with results from limited measurements of dolomite single-isotope diffusion (Anderson, 1972). The calcite Δ_{47} curve is calculated using the optical calcite data and eqn. (14) of Passey and Henkes (2012). No dolomite Δ_{47} reordering parameters are yet published, but clumped isotope measurements of dolomite from the Predazzo contact aureole (Ferry et al., 2011) and the Notch Peak aureole (this study) suggest that it should preserve apparent equilibrium temperatures ~100 °C above calcite. Cooling rates for these data are estimated from a thermal model of the Notch Peak aureole developed in section 6.4, and a similar model reflecting the geometry, depth, and sample location in the Predazzo aureole, and uncertainties therein (Ferry et al., 2002).

Fig. 2: Schematic diagram of the behavior of case-1, 2, and 3 exchange thermometers in a representative thermal metamorphic event. The four key events are 1) peak crystallization, 2) cooling down from peak temperature to the ambient/burial temperature, 3) incubation at ambient temperature, and 4) exhumation to surface. A case-1 thermometer ($T_{peak} < T_c$) records the temperature of peak metamorphism. A case-2 thermometer ($T_{ambient} < T_c < T_{peak}$) records an apparent equilibrium blocking temperature dependent on the cooling rate near this value (T_c). The case-3 ($T_c \leq T_{ambient}$) thermometer fully re-equilibrates with the ambient temperature of the system, and records this value, provided exhumation is rapid enough to quench the system to further exchange.

Fig. 3: Sample locations in the Notch Peak aureole, Utah, USA (modified after Hintze and Davis, 2002)

Fig. 4: Assessment of the accuracy of the bulk $\delta^{13}C$ and $\delta^{18}O$ exchange thermometers. Measured dol-cal fractionations are compared to those predicted from equilibrium crystallization at the temperatures predicted by published thermal models of the Big Horse Ls Member (Table 2). Errors are 2σ standard errors, generated by propagation of mean dolomite and calcite $\delta^{13}C$ or $\delta^{18}O$ errors, assuming dolomite and calcite measurements are uncorrelated (not strictly true, see methods section). Equilibrium temperature-bulk isotope relationships for carbon-13 and oxygen-18 are derived from (Sheppard and Schwarcz, 1970) and (Horita, 2014), respectively.

Fig. 5: Δ_{47} values for calcite and dolomite in the Notch Peak aureole. Errors on individual points are 1σ standard errors of the weighted average of replicates. Blue line is the weighted average of all calcite Δ_{47} measurements in the aureole, with dashed lines denoting the 2σ error envelope on this value. Model peak T values are derived from the equations in (Ferry and Dipple, 1992; Labotka et al., 1988). Dashed gold lines denote the approximate locations of the main metamorphic isograds in the unit. Semitransparent points at 2.63 km are for sample 12-NPK-11b, where abundant secondary cross-cutting carbonate veining has overprinted the primary dolomite and calcite temperature signals (See section 6.2 for details).

Fig. 6: Models for calcite Δ_{47} reordering during cooling in the aureole of the Notch Peak pluton. Calcite apparent equilibrium temperatures approach the ambient temperature of the system during the 100 Ma after intrusion, but whether full re-equilibration occurs depends on the residence temperature and the reordering model used (A). Solid lines were generated using the exchange-diffusion model of Stolper and Eiler (2015), and dotted lines using the first-order approximation model for optical calcite from Passey and Htenkes (2012). Arrhenian parameters were varied by up to 1σ of their reported values and uncertainties to examine the sensitivity of final calcite Δ_{47} temperature to the exact rate constants used (B, C). Symbols are included for clarity, and do not necessarily represent locations where calculations were performed.

Table 1:

Mineral	$\alpha^{13}_{\text{fraction-complete}}$	$\alpha^{13}_{\text{error}}$	$\alpha^{18}_{\text{fraction-complete}}$	$\alpha^{18}_{\text{error}}$
Calcite	0.99999	0.00002	1.00036	0.00003
Dolomite	1.00019	0.00002	1.00026	0.00005

Table 1: Average (n=2-3) fractionation factors for partial recovery of CO_2 from calcite and dolomite during stepped acid digestion procedure. Errors are 1σ standard errors of the fractionations, derived by propagating the standard errors of the replicate measurements of the partial recovery, and complete recovery methods. These measurements are in table EA5. Δ_{47} values of calcite and dolomite standards obtained using the stepped digestion procedure were indistinguishable from their unfractionated values outside of uncertainty, so no corrections were applied.

Table 2:

Sample	Dist (km)	X_dol	# of analyses (Bulk, Cal, Dol)	Calcite (total) $\delta^{13}C$ (vpdb) (‰)	Calcite (total) $\delta^{13}C$ error (‰)	Calcite (total) $\delta^{18}O$ (vpdb) (‰)	Calcite (total) $\delta^{18}O$ error (‰)	Dolomite $\delta^{13}C$ (vpdb) (‰)	Dolomite $\delta^{13}C$ error (‰)	Dolomite $\delta^{18}O$ (vpdb) (‰)	Dolomite $\delta^{18}O$ error (‰)	$T_{13\alpha}$ (°C)	$T_{18\alpha}$ (°C)	T_{model}(°C)	T_{XMg}(°C)	T_{XMg} error (°C)
10H-107	0.09	0.018	3, 4, 2	-0.211	0.013	-10.428	0.048	0.215	0.003	-9.926	0.037	566	408	575		
3H-38a	0.15	0.033	9, 3, 3	0.737	0.009	-10.240	0.033	1.116	0.011	-9.958	0.025	657	537	550	495	17
20H-99	0.58*	0.097	2, 3, 2	0.748	0.009	-9.811	0.049	1.482	0.006	-8.998	0.014	292	299	420	445	11
11H-116	1.88	0.057	6, 1, 4	0.937	0.042	-9.982	0.088	1.662	0.021	-9.443	0.029	297	392	300	248	32
12-NPK-11b	2.63	0.032	2, 1, 2	0.597	0.006	-9.945	0.046	1.460	0.003	-8.962	0.015	237	258	220		
12-NPK-5	4.01	0.030	2, 3, 2	0.692	0.016	-9.755	0.027	1.855	0.008	-8.522	0.020	153	211	170		
12H-122	5.36	0.033	4, 1, 1	0.738	0.043	-10.140	0.131	2.380	0.050	-8.588	0.100	45	166	160		

Table 2: Average values of $\delta^{13}C$ and $\delta^{18}O$ in calcite and dolomite. Reported calcite values (calcite, total) are the unweighted mean of all individual offline calcite digestions and online bulk digestions with the dolomite $\delta^{13}C$ and $\delta^{18}O$ contributions removed (see methods section for details). Errors are 1σ standard errors of the mean of multiple analyses, or the 1σ typical external reproducibility for offline digestion where only one replicate was used (0.05 ‰ and 0.1 ‰ for $\delta^{13}C$ and $\delta^{18}O$, respectively; individual measurements available in the electronic annex). Oxygen-18 and carbon-13 equilibrium fractionation temperatures are calculated using the equations of Horita (2014) and Sheppard and Schwarcz (1970), respectively. Model peak temperatures are from the distance-T relation of Ferry and Dipple (1992), except for sample 12H-122, which is beyond 4 km, where the 4th-order equation is no longer valid. Here, peak temperature was estimated based on the burial depth of the unit and a reasonable upper crustal geotherm (see section 6.3). Actual distance of sample 20H-99 (*) is 0.23 km, however this rock is from a different set of outcrops (in Contact Canyon) than the rest of the sample suite, where isograds are compressed. To more accurately compare sample 20H-99 to the others, it was projected to the distance it would lie at along the main transect in North Canyon.

Table 3:

Sample	Distance (km)	# of analyses (Bulk, Cal, Dol)	Bulk Δ47_ARF (‰)	Bulk Δ47 error (‰)	Calcite Δ47_ARF (‰)	Calcite Δ47 error (‰)	Calcite Δ47 (total) (‰)	Calcite Δ47 (total, error) (‰)	Dolomite Δ47_ARF (‰)	Dolomite Δ47 error (‰)	$T_{\Delta47,cal}$ (°C)(±1σ)	$T_{\Delta47,dol}$ (°C) (±1σ)
10H-107	0.09	3, 4, 2	0.453	0.009	0.451	0.027	0.452	0.015	0.351	0.005	$149.8^{+14.8}_{-13.2}$	$312.7^{+15.0}_{-13.9}$
3H-38a	0.15	9, 3, 3	0.443	0.005	0.444	0.020	0.446	0.006	0.340	0.006	$155.5^{+6.0}_{-5.7}$	$347.6^{+22.3}_{-19.9}$
20H-99	0.58*	2, 3, 2	0.426	0.005	0.420	0.020	0.426	0.012	0.341	0.010	$176.8^{+14.8}_{-13.2}$	$344.2^{+37.9}_{-31.5}$
11H-116	1.88	6, 1, 4	0.453	0.011	0.430	0.014	0.456	0.011	0.359	0.013	$146.2^{+10.4}_{-9.5}$	$291.0^{+36.7}_{-30.1}$
12-NPK-11b	2.63	2, 1, 2	0.469	0.007	0.465	0.013	0.467	0.005	0.458	0.007	$136.6^{+4.2}_{-4.1}$	$144.4^{+6.4}_{-6.1}$
12-NPK-5	4.01	2, 3, 2	0.440	0.011	0.434	0.013	0.435	0.009	0.402	0.004	$166.8^{+10.0}_{-9.3}$	$208.2^{+6.0}_{-5.8}$
12H-122	5.36	4, 1, 1	0.475	0.013	0.445	0.010	0.467	0.011	0.439	0.016	$136.6^{+9.5}_{-8.8}$	$162.6^{+17.8}_{-15.5}$

Table 3: Average Δ_{47} values of online bulk powder measurements, and offline calcite, dolomite digestions. Total calcite values were obtained by averaging all offline measurements of calcite fractions and online bulk measurements with the dolomite contribution removed (see methods section for details). Errors in bulk, calcite, total calcite, and dolomite Δ_{47} values are 1σ standard errors of the mean of multiple analyses, or 1σ measurement errors where only one replicate was used. The Δ_{47}-temperature calibration is based on a second-order polynomial fit in Δ_{47} vs. $1/T^2$-space to the data of Ghosh et al. (2006), Guo et al. (2009), Boniface et al., (2011), and Stolper and Eiler (2015) (see methods for details). Actual distance of sample 20H-99 (*) is 0.23 km, however this rock is from a different set of outcrops (in Contact Canyon) than the rest of the sample suite, where isograds are compressed. To more accurately compare sample 20H-99 to the others, it was projected to the distance it would lie at along the main transect in North Canyon.

Table 4:

Parameter	Value	Units	Description	Source
T0	1173	K	initial monzonite temperature	Nabelek (2009)
dT/dz	0.025	K/m	geothermal gradient in limestones	Nabelek (2009)
ρ_l	2700	kg/m3	density of limestone	Ahrens (1995)
ρ_m	2700	kg/m3	density of monzonite	Ahrens (1995)
A_l	0.3	μW/m3	radiogenic heat production of limestone	Wollenberg (1987)
A_m	0.7	μW/m3	radiogenic heat production of monzonite	Wollenberg (1987)

Thermal diffusivity equation
$\kappa = 0.534 + 5.017*e\text{-}T/222.1$

Table 4: Description of the values used to numerically solve the thermal diffusion equation in the model Notch Peak aureole.

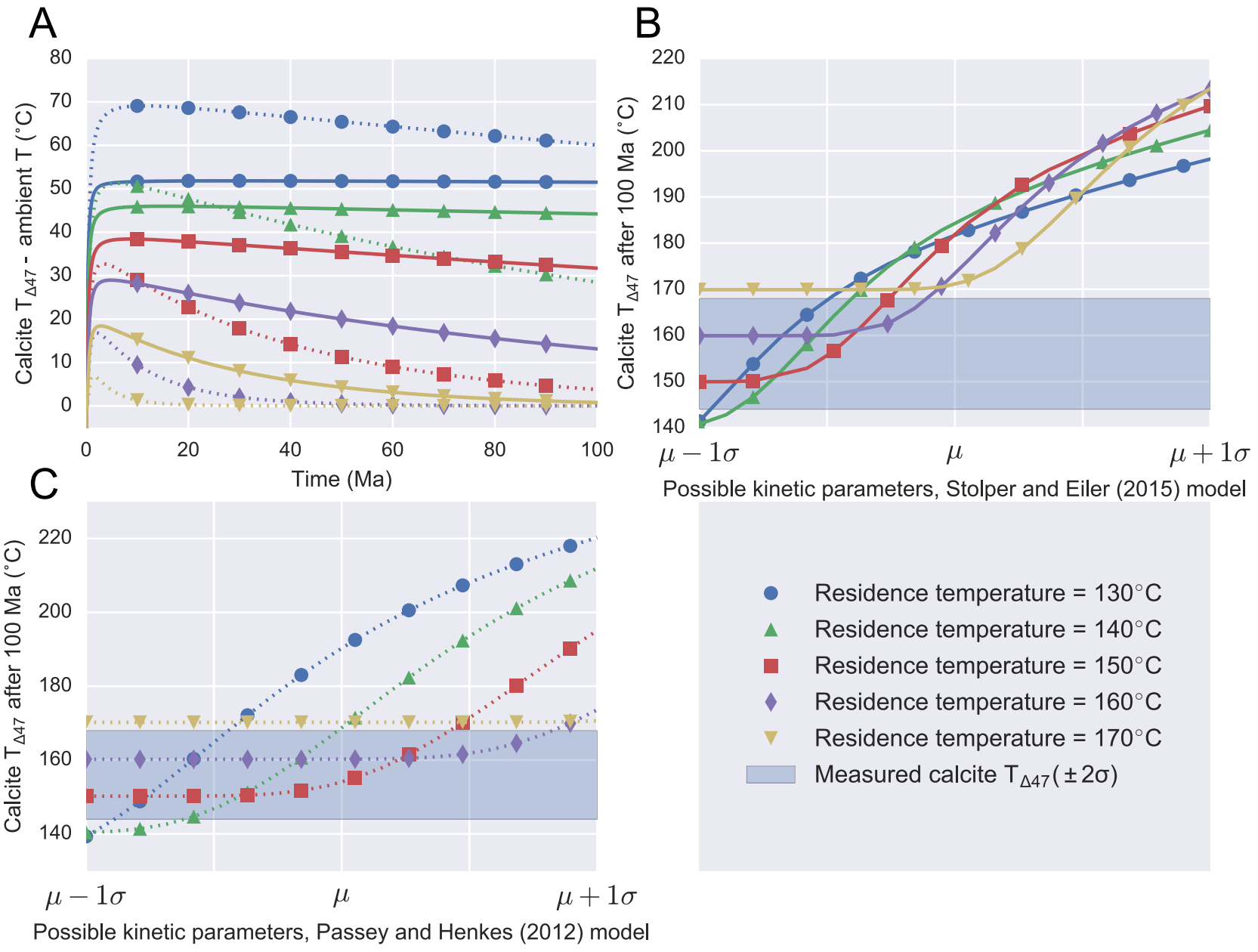
A
Calcite $T_{\Delta47}$ - ambient T (°C)
Time (Ma)
B
Calcite $T_{\Delta47}$ after 100 Ma (°C)
$\mu - 1\sigma$
μ
$\mu + 1\sigma$
Possible kinetic parameters, Stolper and Eiler (2015) model
C
Calcite $T_{\Delta47}$ after 100 Ma (°C)
$\mu - 1\sigma$
μ
$\mu + 1\sigma$
Possible kinetic parameters, Passey and Henkes (2012) model
Residence temperature = 130°C
Residence temperature = 140°C
Residence temperature = 150°C
Residence temperature = 160°C
Residence temperature = 170°C
Measured calcite $T_{\Delta47}$ (±2σ)

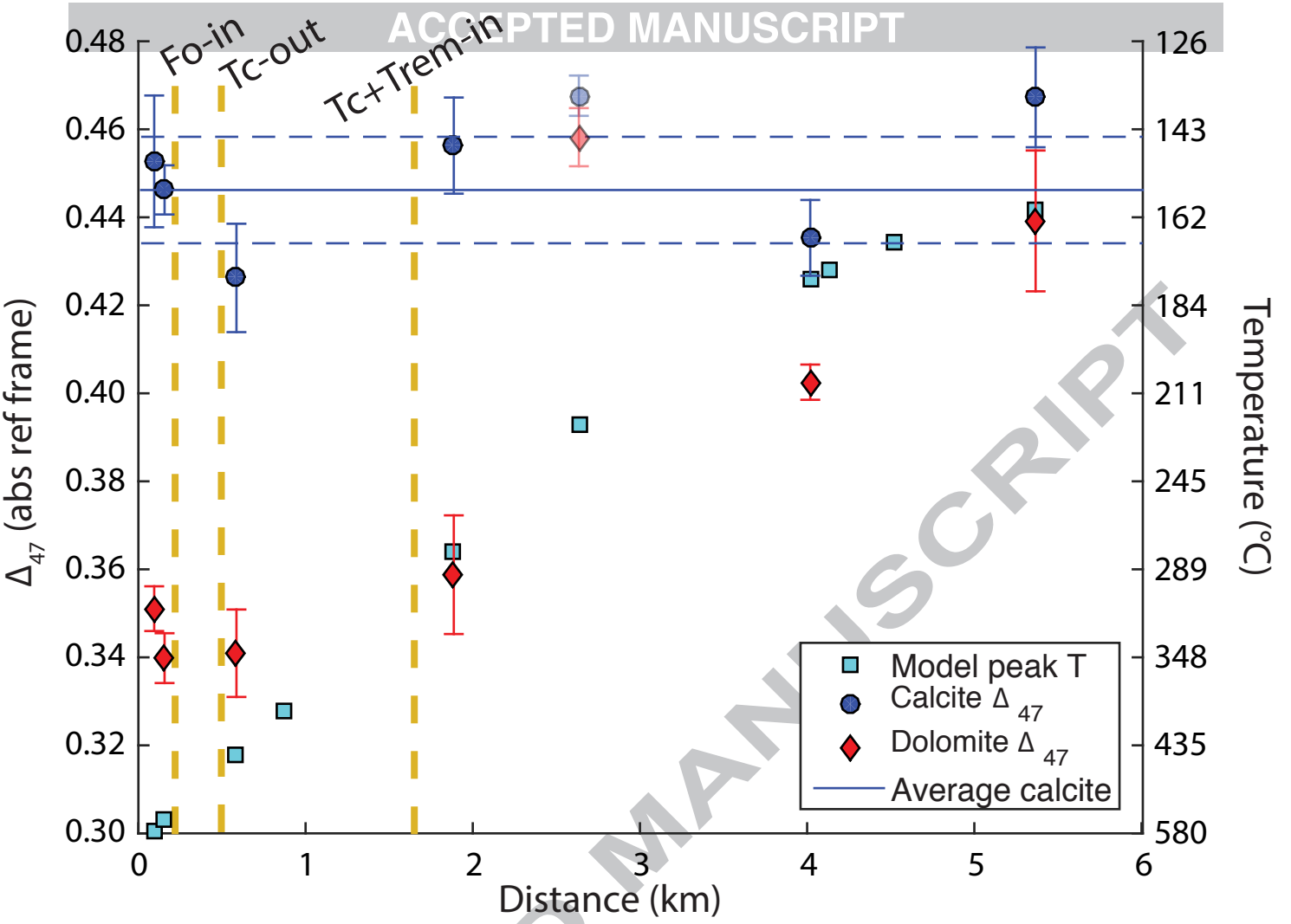

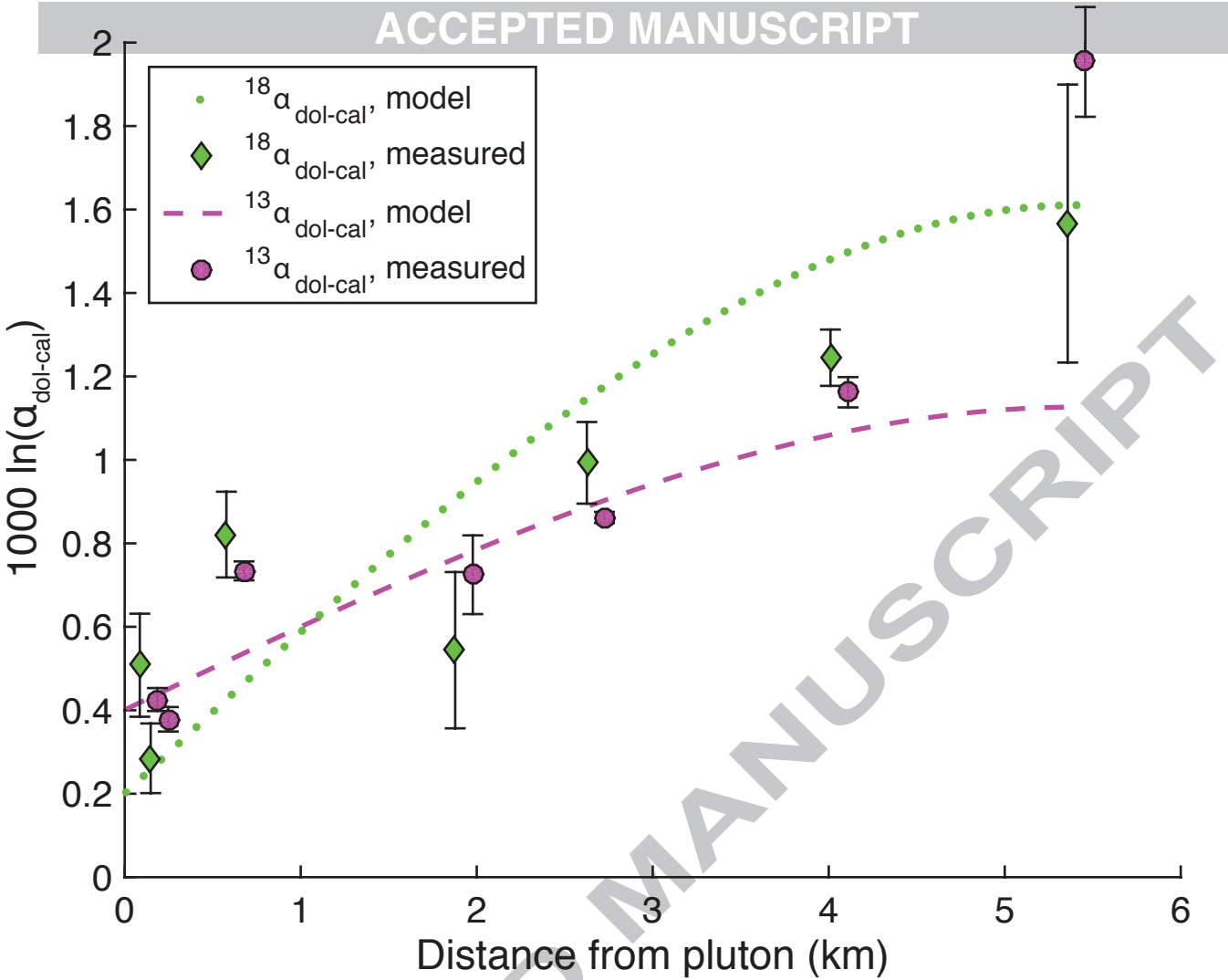

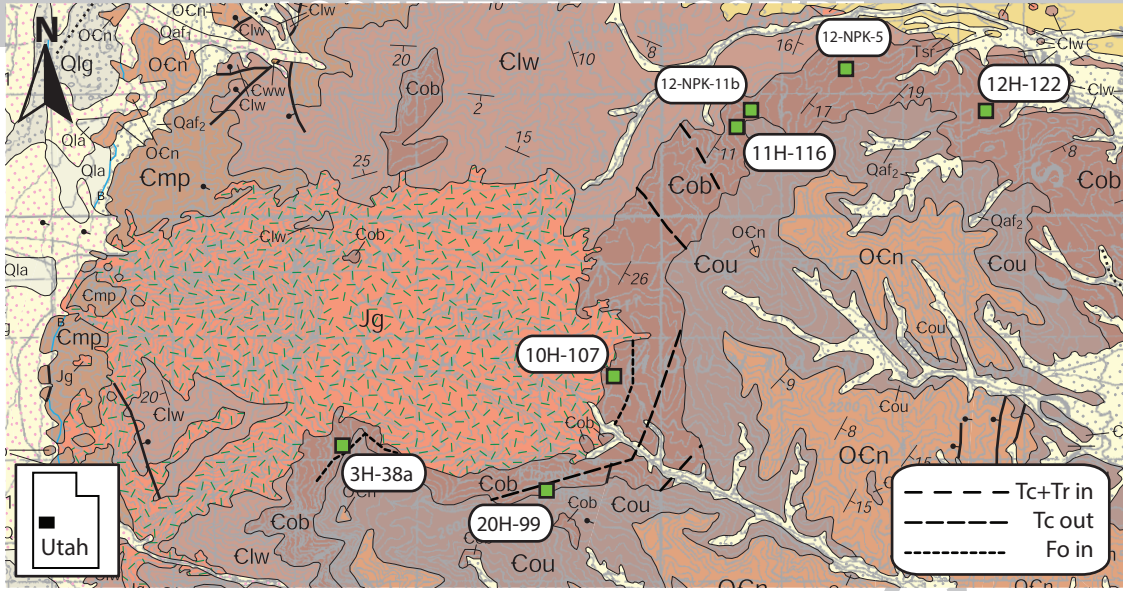
N
Qlg
OCn
Qaf1
Clw
Cww
Qaf2
Qla
Cmp
B
Jg
Cob
20
25
2
15
10
8
16
12-NPK-5
Tsr
12-NPK-11b
11H-116
12H-122
19
17
11
Qaf2
Cou
26
9
10H-107
3H-38a
20H-99
Utah
Tc+Tr in
Tc out
Fo in
2 km

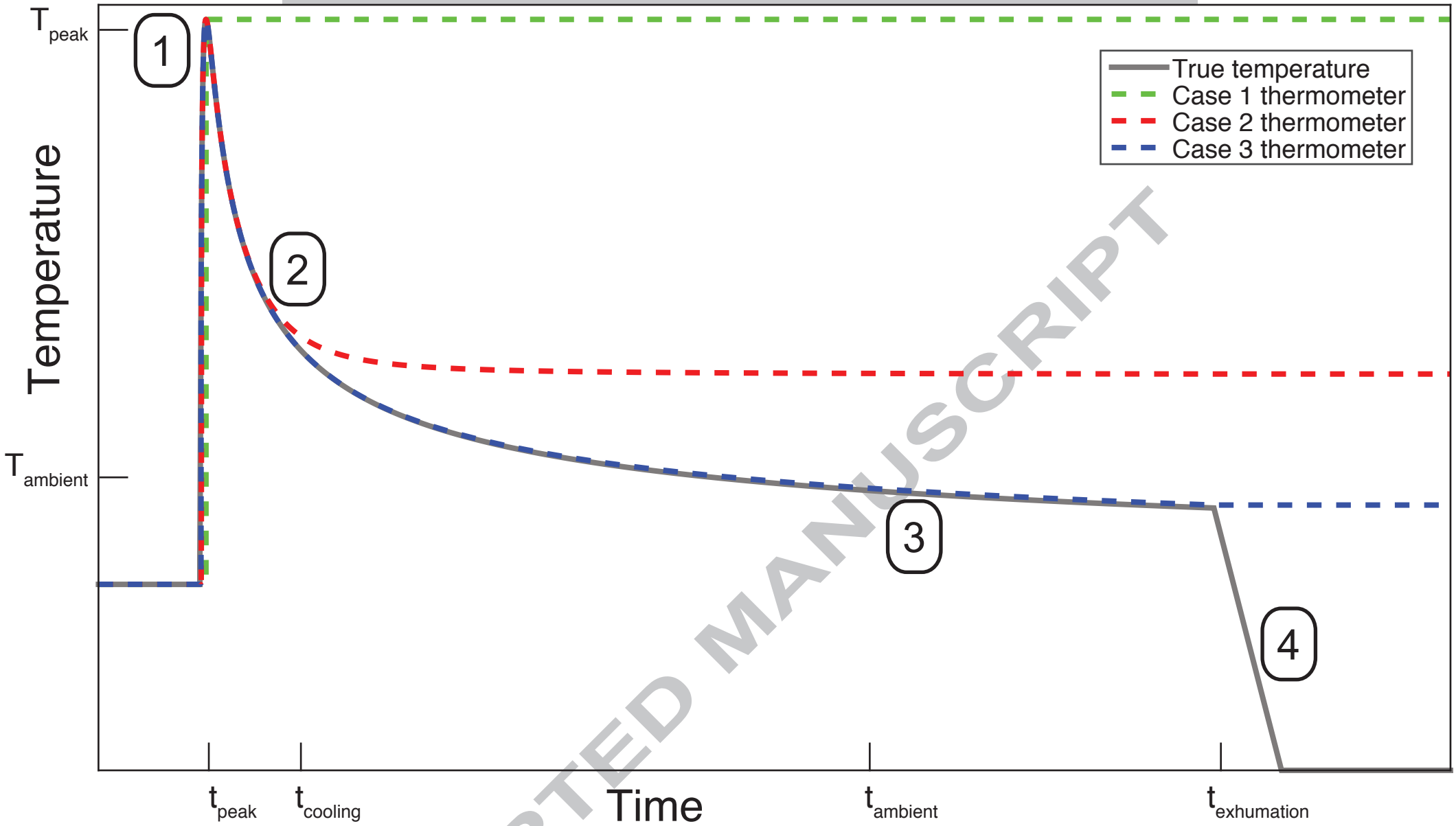

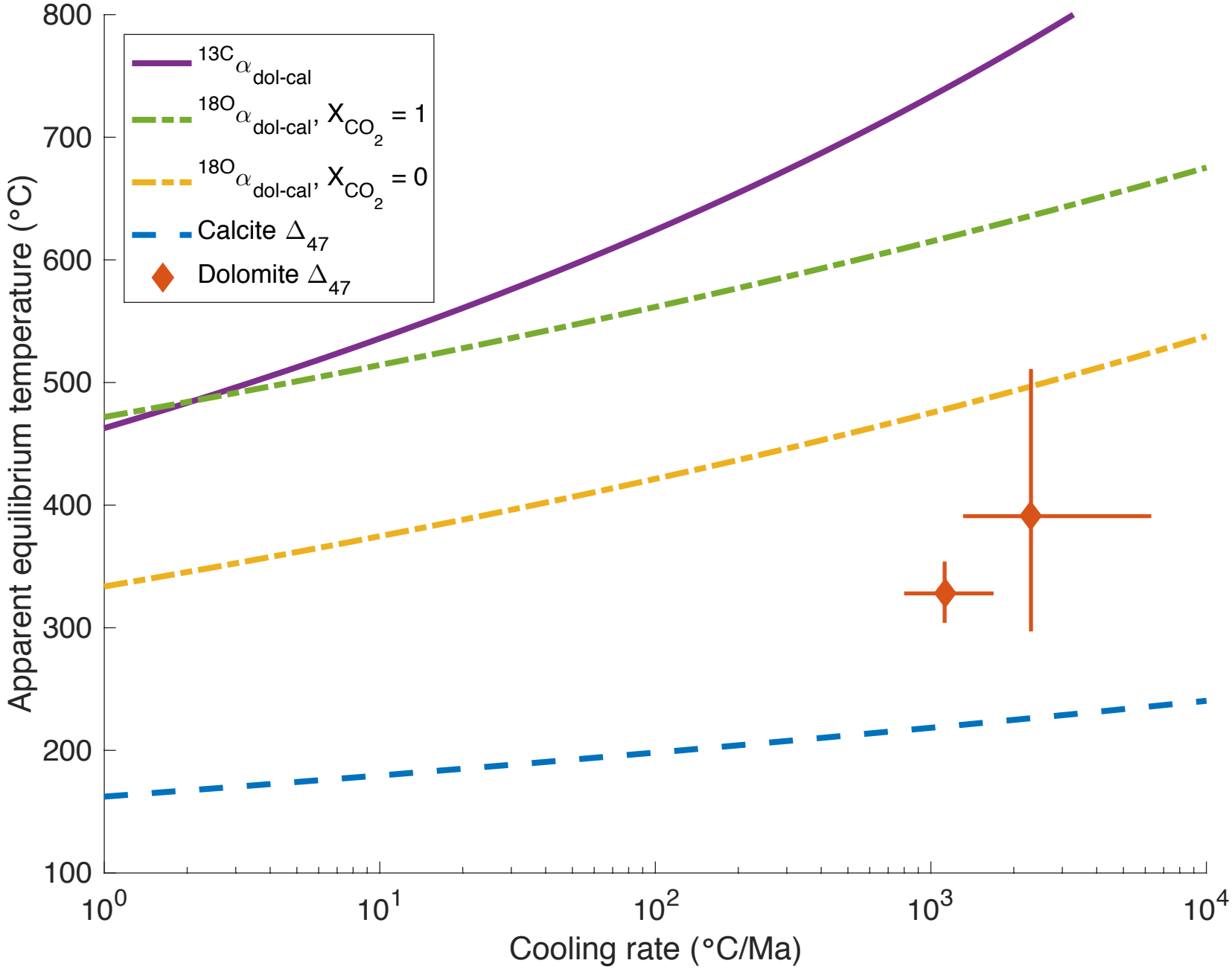
800
700
600
500
400
300
200
100
Apparent equilibrium temperature (°C)
10^0
10^1
10^2
10^3
10^4
Cooling rate (°C/Ma)
$^{13C}\alpha_{dol\text{-}cal}$
$^{18O}\alpha_{dol\text{-}cal}$, X_{CO_2} = 1
$^{18O}\alpha_{dol\text{-}cal}$, X_{CO_2} = 0
Calcite Δ_{47}
Dolomite Δ_{47}